ABSTRACT

Title of Thesis: CRITICAL IGNITION CONDITIONS OF STRUCTURAL MATERIALS BY CYLINDRICAL FIREBRANDS
Hamed Salehizadeh, Master of Science, 2019

Thesis Directed By: Professor Michael J. Gollner
Department of Fire Protection Engineering

Smoldering firebrands (embers) are a major cause of ignition and eventual structural damage during wildfires at the wildland-urban interface (WUI). These small pieces of wood can loft several kilometers ahead of the main flame front and ignite spot fires directly on structural elements such as decks. In this research, dense structural materials such as wood and engineered wood will be studied with a focus on capturing the critical thermal conditions necessary for ignition. Unique to this study will be a configuration where whole piles of firebrands are placed on the recipient material, emulating observations from WUI fires. In order to design appropriate fire safety standards at the WUI and, someday, to model the propagation of these fires, the conditions leading to ignition of common WUI materials by piles of lofted firebrands must be quantified.

Firebrands were modeled using small cylindrical wooden dowels which were ignited and placed in a small-scale wind tunnel. Two tests were performed for each loading condition of firebrands, one studying ignition of wooden structural elements such as decking and marine-grade plywood and another measuring temperatures and heat fluxes over an inert piece of ceramic insulation. A single-point water-cooled heat flux gauge was used for time-resolved measurements of heat flux at the center of the inert setup surrounded by thin-skin calorimeters and K-type thermocouples which allowed for a spatial characterization of heating. The wind speed was the main quantity of interest changed during the test to determine the effects of wind speed on the heat flux released from the glowing dowels to recipient fuels. The results showed a drastic increase in heating from piles of firebrands vs. individual brands. The piles also produced higher heat fluxes under increasing winds. This is due, for the most part, to higher surface temperatures resulting from increased surface oxidation under higher wind speeds. Both smoldering and flaming ignition of wood was found to be similarly dependent on wind speed. Larger piles also produced higher peak heat fluxes at the center of the pile, highlighting the role of re-radiation within the pile influencing heat fluxes to recipient fuels. Critical heat flux and firebrand loading conditions required to achieve smoldering and flaming ignition of structural materials used in the WUI are determined by comparing tests with inert and flammable fuels.

These critical conditions can be used to model the propagation of WUI fires over structural elements to design appropriate fire safety standards at the WUI. A non-dimensional relationship incorporating fuel type, geometry, and ambient conditions is also proposed to describe the results.

CRITICAL IGNITION CONDITIONS OF STRUCTURAL MATERIALS BY CYLINDRICAL FIREBRANDS

by

Hamed Salehizadeh

Thesis submitted to the Faculty of the Graduate School of the
University of Maryland, College Park in partial fulfillment
of the requirements for the degree of
Master of Science
2019

Advisory Committee:
Associate Professor Michael J. Gollner, Chair
Professor Arnaud Trouve
Associate Professor Stanislav Stoliarov

Acknowledgments

I would like to thank many people helping me during this project. First, I would like to thank Dr, Michael Gollner, my academic advisor who supported me and helped me in this project and during my master's studies. I had a wonderful two years of experience working in his research group as a graduate research assistant. I also would like to thank my committee members, Dr. Arnaud Trouve and Dr. Stanislav Stoliarov for their time and reviewing my thesis as well as their useful comments on my thesis. It was my pleasure working with many undergraduate students during this project. I would like to thank Jessen Oey, Max Scott, Alison Davis and Michael Jones for helping me in the experiments. I also would like to thank Raquel Hakes who helped me to learn many things in the lab when I joined the project. I was really fortunate to study fire protection engineering at University of Maryland and would like to thank all professors and staffs in the department for their support. I am grateful to Brian Sullivan who helped me to provide and buy all materials required for the experiments. I am also grateful to all of my research group members who helped me in the lab and I had wonderful time with them in past two years. I also would like to thank NIST staff for their support and consideration in this project. I would like to thank NIST for funding this project and my master's studies. At the end, I would like to thank my family specially Parisa, my beloved wife, who always

supported me. Thank you so much.

Table of Contents

1.1 Motivation 4
1.2 Objectives 6
2.1 Overview 8
2.2 Smoldering and Flaming 9
2.3 Ignition of Vegetative Fuels 11
2.4 Ignition of Dense Fuels 14
3.1 Overview of Experiments 17
3.2 Firebrand Production 17
3.3 Wind Tunnel 19
3.4 Thermal Sensor Array 20
3.5 Ignition Tests 22
3.6 Calibration 25
3.6.1 Water-Cooled Heat Flux Gauge 25
3.6.2 Thinskin Calorimeters 27
3.6.3 Wind Speed 31
4.1 Summary 34
4.2 Time-resolved Heat Flux 34
4.3 Total Thermal Energy Transport 54
4.4 Temperature Measurements 57
4.5 Ignition Results 65
4.5.1 Time to Smoldering 66
4.5.2 Critical Heat Flux at Smoldering 68
4.5.3 Time to Flaming 70
4.5.4 Critical Heat Flux at Flaming 73
5.1 Wind Effects 75
5.2 Scaling Analysis 76
5.2.1 Smoldering Condition 76
5.2.2 Flaming Condition 79
6.1 Summary 82
6.2 Conclusion 82
6.3 Future Work 83
7.1 Heat flux Results 85
7.2 TSC data 87
7.3 Few samples of Ignition Tests Results-TC data 101
7.4 Table of all tests performed 106

List of Figures

2.1 Schematic of heat transfer between a firebrand and a fuel bed. 9
2.2 Ignition propensity of dry cellulose using heated steel spheres. This figure shows the quality of ignition depend on particle size and temperature [1] 11
2.3 Flaming in the corner assemblies were additional fuel was presented. Also firebrand generated from fences can be seen. (From [2] 14
3.1 Schematic of the experimental setup showing a wind tunnel, sensor array, and burner in a side view. 20
3.2 Schematic showing sensor WC-HFG and TSC locations over an inert board. Four inner TSCs and 12 outer TSCs are indicated, later used to distinguish temperatures near the center and edge of firebrand piles. 22
3.3 Schematic showing a side-view of a wooden sample used during igntition tests. Thermocouples are labeled TC1 to TC5. 23
3.4 The top figure shows TC measurements at 5 locations along the centerline of a plywood fuel sample. The bottom figure shows a corresponding side-view photograph of the centerline o the cut sample used to determine threshold for smoldering ignition. Two holes for thermocoupels on the left-hand side are still visible, while the others have deformed and are no longer visible. 25
3.5 Temperatures from TCs and TSCs with 16 g of firebrands deposited over a sensor array under a wind speed of 0.5 m/s. Each solid line represents temperatures from TSCs or TCs averaged between 5 repeated tests over 5 locations. The shaded area represents the standard deviation between the tests and locations, with TSCs having slightly less variability. 28
3.6 Temperatures from TCs and TSCs with 16 g of firebrands deposited over a sensor array under a wind speed of 0.8 m/s. Each solid line represents temperatures from TSCs or TCs averaged between 5 repeated tests over 5 locations. The shaded area represents the standard deviation between the tests and locations, with TSCs having slightly less variability. 29
3.7 Temperatures from TCs with 16 g of firebrands deposited over a sensor array under a wind speed of 0.5 m/s. 30
3.8 Temperatures from TCs with 16 g of firebrands deposited over a sensor array under a wind speed of 0.8 m/s. 31

3.9 Wind speeds measured at different heights above the surface of the wind tunnel with an average wind speed from 0.5 m/s to 3.5 m/s. The solid lines show the wind profiles measured before depositing firebrands and dashed lines show wind profile with firebrands deposited. 32
3.10 Photographs showing the methodology used to measure wind speeds including the tip of the hot-wire anemometer (right) and wind speed measurements being performed with a simulated presence of firebrands (left). 33
4.1 Heat fluxes recorded from a WC-HFG are shown with 16 g of smoldering birch firebrands deposited over the sensor under different wind speeds. 35
4.2 The probability of flame appearance over smoldering firebrands during experiments over an inert substrate. 38
4.3 The heat flux from WC-HFG data when 8 g smoldering birch firebrands were deposited over sensors in different wind speeds. Shaded area shows standard deviation for all tests have been done which birch from vendor 1. The wind speed is 0.5 m/s in the top-left graph, 0.8 m/s in the top-right graph, 1.2 m/s in the bottom-left graph and 1.4 in bottom-right graph.. 40
4.4 The heat flux from a WC-HFG when 4 g of smoldering birch firebrands were deposited over sensors in different wind speeds. The shaded area shows the standard deviation for all tests. The wind speed is 0.5 m/s in the top-left graph, 0.8 m/s in the top-right graph, 1.2 m/s in the bottom-left graph and 1.4 in bottom-right graph. Note the firebrands are made of birch wood from vendor 1. 41
4.5 The average heat flux from a WC-HFG when 4, 8 and 16 g of smoldering birch firebrands were deposited over inert sensors under different wind speeds. The deposited mass starts at 4 g in the top-left graph, 8 g in the top-right graph and 16 g in the bottom-right. 42
4.6 Peak heat fluxes from a WC-HFG for different firebrand mass loading and wind speeds. 44
4.7 Side view photo from a pile with a deposited mass of 4g. 48
4.8 Side view photo from a pile with a deposited mass of 8g. 49
4.9 Side view photo from a pile with a deposited mass of 16g. 49
4.10 The bulk density of pile with respect to its deposited mass. 50
4.11 WC-HFG measurements of heat flux for 8 g of different firebrand types under a wind speed of 0.5 m/s. Heat fluxes shown are an average between at least 3 repeated tests. 51

4.12 Peak heat fluxes extracted from WC-HFG measurements for an 8 g mass of firebrands from three different fuels deposited onto an inert sensor array under a 0.5 m/s wind. Peak heat fluxes were determined as the highest value over time along a curve averaged between repeated tests. 53
4.13 The total energy transferred from firebrands to an inert fuel bed is shown as a function of wind speed. 55
4.14 The total energy transferred from firebrands to an inert fuel bed is shown as a function of density for three fuel samples. All tests had 8 g of firebrands deposited over sensors under a wind speed of 0.5 m/s . 56
4.15 Temperatures recorded from TSC sensors in both inner (TSC1) and outer (TSC2) locations below a pile of 4 g of firebrands under different wind speeds. 58
4.16 Temperatures recorded from TSC sensors in both inner (TSC1) and outer (TSC2) locations below a pile of 8 g of firebrands under different wind speeds. 59
4.17 Temperatures recorded from TSC sensors in both inner (TSC1) and outer (TSC2) locations below a pile of 16 g of firebrands under different wind speeds. 60
4.18 Peak Inner and Outer TSC temperatures when 16, 8 and 4 g firebrand deposited for different tests with birch (vendor 1). The peaks were collected from figures 4.15, 4.16 and 4.17. These values are presented on separate graphs for each deposited mass in the appendix 61
4.19 Temperatures measured from an array of TSCs presented at $t = 200$ s for 16 g of initial deposited firebrand mass under a wind speed of 0.8 m/s. 62
4.20 Temperatures measured from an array of TSCs presented at $t = 200$ s for 16 g of initial deposited firebrand mass under a wind speed of 1.4 m/s. 63
4.21 Temperatures measured from an array of TSCs presented at $t = 200$ s for 16 g of initial deposited firebrand mass under a wind speed of 1.4 m/s 64
4.22 Time to smoldering calculated using an in depth thermocouple for three fuel samples, marine grade plywood (MGP), oriented strand board (OSB) and cedar wood. 67
4.23 Critical heat fluxes estimated at the onset of smoldering. 69

4.24 Time to flame observed from videos. Each average is taken from at least 5 repeated tests. The color-shaded propensity shows the percentage that flaming occurred. In all tests, 16 grams of firebrands were deposited. 71
4.25 Transition from smoldering to flaming of the fuel bed. 72
4.26 Photograph showing flames present both over the pile of firebrands and over the fuel surface. 73
4.27 Critical heat flux determined at the time to flaming. 74
5.1 Experimental data fitted on scaling analysis 78
5.2 Experimental data fitted on scaling analysis 80
5.3 Experimental data fitted on scaling analysis 81
7.1 Average heat flux for different deposited mass when wind speed is 0.5 m/s 85
7.2 Average heat flux for different deposited mass when wind speed is 0.8 m/s 86
7.3 Average heat flux for different deposited mass when wind speed is 1.2 m/s 86
7.4 Average heat flux for different deposited mass when wind speed is 1.4 m/s 87
7.5 TSC data for wind speed of 0.5 m/s when 4 g firebrand were deposited. 87
7.6 TSC data for wind speed of 0.5 m/s when 8 g firebrand were deposited. 88
7.7 TSC data for wind speed of 0.5 m/s when 16 g firebrand were deposited. 88
7.8 TSC data for wind speed of 0.8 m/s when 4 g firebrand were deposited. 89
7.9 TSC data for wind speed of 0.8 m/s when 8 g firebrand were deposited. 89
7.10 TSC data for wind speed of 0.w m/s when 16 g firebrand were deposited. 90
7.11 TSC data for wind speed of 1.2 m/s when 4 g firebrand were deposited. 90
7.12 TSC data for wind speed of 1.2 m/s when 8 g firebrand were deposited. 91
7.13 TSC data for wind speed of 1.2 m/s when 16 g firebrand were deposited. 91
7.14 TSC data for wind speed of 1.4 m/s when 4 g firebrand were deposited. 92
7.15 TSC data for wind speed of 1.4 m/s when 8 g firebrand were deposited. 92
7.16 TSC data for wind speed of 1.4 m/s when 16 g firebrand were deposited. 93
7.17 Peak inner and outer temperature from average TSC data for each wind speed when 4 g firebrand is deposited over fuel. 94

7.18 Peak inner and outer temperature from average TSC data for each wind speed when 8 g firebrand is deposited over fuel. 94
7.19 Peak inner and outer temperature from average TSC data for each wind speed when 16g firebrand is deposited over fuel. 95
7.20 TSC data for wind speed of 0.5 m/s when 4 g firebrand were deposited. 95
7.21 TSC data for wind speed of 0.5 m/s when 8 g firebrand were deposited. 95
7.22 TSC data for wind speed of 0.5 m/s when 16 g firebrand were deposited. 96
7.23 TSC data for wind speed of 0.8 m/s when 4 g firebrand were deposited. 96
7.24 TSC data for wind speed of 0.8 m/s when 8 g firebrand were deposited. 97
7.25 TSC data for wind speed of 0.8 m/s when 16 g firebrand were deposited. 97
7.26 TSC data for wind speed of 1.2 m/s when 4 g firebrand were deposited. 98
7.27 TSC data for wind speed of 1.2 m/s when 8 g firebrand were deposited. 98
7.28 TSC data for wind speed of 1.2 m/s when 16 g firebrand were deposited. 99
7.29 TSC data for wind speed of 1.4 m/s when 4 g firebrand were deposited. 99
7.30 TSC data for wind speed of 1.4 m/s when 8 g firebrand were deposited. 100
7.31 TSC data for wind speed of 1.4 m/s when 16 g firebrand were deposited. 100
7.32 TC data for plywood when 16 g firebrands were deposited and wind speed was 0.8 m/s. 101
7.33 TC data for plywood when 16 g firebrands were deposited and wind speed was 1 m/s. 101
7.34 TC data for Cedar when 16 g firebrands were deposited and wind speed was 0.8 m/s. 102
7.35 TC data for Cedar when 16 g firebrands were deposited and wind speed was 0.5 m/s. 102
7.36 TC data for Cedar when 16 g firebrands were deposited and wind speed was 0.8 m/s. 103
7.37 TC data for OSB when 16 g firebrands were deposited and wind speed was 0.5 m/s. 103
7.38 TC data for OSB when 16 g firebrands were deposited and wind speed was 0.8 m/s. 104
7.39 TC data for OSB when 16 g firebrands were deposited and wind speed was 1.2 m/s. 104

Chapter 1: Introduction

Over the past few decades, losses from fires at the wildland-urban interface (WUI) have increased dramatically [3]. The WUI is an area where houses and human development are mixed within wildland vegetation [4]. This may occur when individual structures are placed within broader undeveloped lands (intermix) or at the edge of a suburban development (interface), but regardless represents a confluence of structures and surrounding flammable vegetation. Increasing losses from fires in these areas can be described by considering three factors. First, an increasing population has been moving into WUI areas as suburban developers look for additional land and the draw of a less-dense environment brings more people. The growth of structures in these areas, many of which used to experience normal fire intervals, both exposes a greater population to these fires than in the past and contributes to an increased number of accidental ignition sources [5]. Second, land management practices have generally removed fire from the landscape, extinguishing small fires soon after they are started. The result is a build-up of fuel that eventually burns under the hottest and driest conditions, where any type of fire suppression is unlikely to have an effect. Finally, climate change has been linked to an increase in the number of hot, dry days following long droughts [6]. An increase in these fire danger conditions increases the likelihood that devastating wildland fires can occur.

Recent incidents have shown that the trend of devastating WUI fires is getting worse. Table 1 shows several recent fires, including the number of structures destroyed and potential financial losses. Notable fires include the December 2017 Thomas fire, which became the largest wildfire in California's history and the 2017 Tubbs, Atlas and Nuns fires in Northern California, which destroyed over 5600 structures, killed 22 people and caused over 2 billion dollars (US) in damage. More recently, the 2018 Camp fire became the deadliest and most destructive wildfire in California's history, destroying over 18,000 structures, killing 85 civilians, and causing 16 billion dollars (US) in damage. The wildfire problem is not only a California problem, devastating WUI fires have occurred in Tennessee (Gatlinburg, 2016), Greece, Spain, Portugal and Canada. One method of reducing losses from these fires is to harden structures so that they become more resistant to fire. [7, 8].

Table 1: Top 10 Most Destructive Wildfires in California				
Fire Name	Date	Area (acres)	Structures Destroyed	Fatalities
Camp Fire	November 2018	153,336	18,804	85
Tubbs	October 2107	36,807	5,636	22
Tunnel	October 1991	1,600	2,900	25
Cedar	October 2003	273,246	2,820	15
Valley	September 2015	76,067	1,955	4
Witch	October 2007	197,990	1,650	2
Woolsey	November 2018	96,949	1,643	3
Carr	July 2018	229,893	1,614	8
Nuns	October 2017	54,382	1,355	3
Thomas	December 2017	281,893	1,063	2

The ignition of structures by wildfires occurs due three types of exposure conditions [3]. First, radiation was long thought to be responsible for most structure ignitions. Largely due to work by Cohen, it was found that even large flames from crown fires have a difficult time igniting structural materials when flames are more than 20-30 m from the structure [9]. When the area around a home is cleared an appropriate distance to prevent radiative ignition, termed defensible space, ignition

of structures by radiation from approaching wildfires can be avoided. The exception are cases where urban conflagrations arise, and fires can spread from home-to-home, both by radiation and firebrands.

Firebrands are small pieces of burning embers (usually wooden materials) generating from burning trees, vegetation and other materials during wildland fires. Previous investigations have shown that firebrands are a major cause of structure losses during WUI fires, igniting structures and secondary fires far away from the main fire front [10]. During these fires, firebrands have been found to ignite fuels several kilometers away from the fire, complicating suppression efforts. While early works by Cohen [6] and numerous investigations by Maranghides [11], have shown that firebrands are a major source of structural losses, our understanding of the physical mechanisms by which firebrands generate, loft, and eventually ignite structures is still in its early stages [3].

1.1. Motivation

While several studies have investigated the role that one or several individual firebrands play on the ignition of a structural component, many times whole piles of firebrands may land on an area prior to ignition, especially in crevices or corners [11, 12]. Most detailed ignition studies have focused on low density vegetative fuel beds, typifying wildland fuels, which may behave different than dense materials such

as wooden structural or architectural elements used on residential homes.

Hakes et al. [13, 14] recently studied heat fluxes from a pile of firebrands made up of wooden cylinders with variable diameters and masses onto a dense wooden material, finding that larger pile sizes increased rates of heating while the effect of firebrand diameter was relatively negligible. Most tests were performed under ambient conditions; however, one test was performed at a higher wind speed, which presented a dramatic increase in heating and reduction in the time to ignition of the tested fuel. With wind speed playing such an important role, it is desired for a range of wind speeds to be studied. The effect of different materials, both for the firebrand and fuel bed, are also of interest.

In order to design appropriate fire safety standards at the WUI and, someday, to model the propagation of these fires, the conditions leading to ignition of common WUI materials by piles of lofted firebrands must be quantified. The goal of this work is to apply the new methodology used by Hakes et al. [14] to measure heat fluxes from piles of firebrands to various wind conditions and understand how these conditions relate to those which cause flaming and smoldering ignition of various WUI materials.

The configuration chosen is still a flat surface which, while somewhat unrealistic, is simple and repeatable as a range of effects such as wind speed and material prop-

erties are studied. Later experiments are planned incorporating different geometries, such as crevices, on the fuel. Other simplifications, such as using oven-dried fuels, remove effects such as moisture content. Fuels, however, often are not moist during the most severe fire danger conditions, with these results representing a worst-case scenario. The effects of wind, which are critical in increasing the rate of oxidation occurring in smoldering firebrands, will be investigated and is found to play an important role.

1.2. Objectives

As discussed, the main goal of this study is to quantify the ignition conditions of dense fuels, such as structural elements, upon firebrand attack. In order to capture these critical conditions, firebrands were studied as a pile and deposited over several different common WUI fuels. Both pile deposited mass and wind speed were varied during experiments. The study is conducted in three parts.

First, in order to understand heating from a pile of firebrands, the heat transferred from glowing firebrands to fuel beds is quantified over an inert sample. Heat fluxes, surface temperatures, and a spatial heating map below the smoldering firebrand pile are measured in a newly-designed experimental apparatus. The effect of wind speed, firebrand deposited mass, and firebrand type are then varied.

Ignition conditions for real fuels are also determined and quantified. For flaming

ignition conditions, the time that it takes for flames to appear over the surface of the fuel bed is chosen to quantify flaming ignition. For smoldering ignition, a vertical smoldering propagation rate from the surface to the half-thickness of the fuel, measured with embedded thermocouples, is used to deduce a smoldering ignition time. The effects of fuel density and wind speed on smoldering and flaming is determined.

Finally, measured heat fluxes and temperatures of firebrands are compared with ignition conditions, connecting thermal conditions with the potential for ignition of the fuel beds. A non-dimensional correlation is presented to represent ignition probability as a factor of firebrand deposited mass, wind speed, density of fuel, density of firebrands, and fuel bed geometry.

Chapter 2: Literature Review

2.1. Overview

The goal of this research is to quantify the critical conditions necessary to ignite WUI fuels. In this chapter, previous studies related to ignition of fuels by firebrands, heat transfer between firebrands and fuel beds, ignition theories, and differences between smoldering and flaming combustion will be reviewed.

Heat transfer between a pile of firebrands and a fuel bed is a complex phenomena related to many factors such as firebrand mass, geometry, type, and ambient wind speed. In a simplified view, displayed in Figure 2.1 this heat transfer can be thought of occurring when a temperature difference exists between glowing firebrands and a cold fuel bed. If there is relatively good contact between the firebrand and the fuel bed, heat will most likely transfer via conduction. If there is poor contact, radiation may play a larger role.

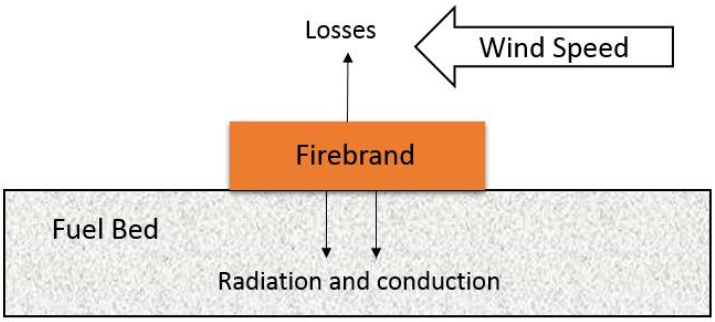

Figure 2.1: Schematic of heat transfer between a firebrand and a fuel bed.

Studying the quantity of heat transferred, the time over which it takes to transfer, and the mode by which this heat is transferred are all important in development of a model for firebrand ignition. Ultimately, how much heat is needed for ignition of a particular fuel bed must be determined.

2.2. Smoldering and Flaming

When glowing firebrands are deposited over a fuel bed, they must provide a sufficient quantity of heat to raise the temperature of enough of the fuel so that a sustained oxidation or pyrolysis reaction occurs. Typically, ignition in wooden fuels starts as a smoldering phase of combustion. Smoldering is a slow solid-phase oxidation process also termed glowing combustion. The peak temperature of smoldering combustion is much lower than flaming combustion, with reactions occurring in the

solid, rather than the gas phase [15]. Initiation of smoldering combustion also requires a much lower critical heat flux, from 8-9 kW/m^2 for smoldering vs. 32-37 kW/m^2 for flaming ignition of a polyurethane foam sample [1, 16].

If a solid material is sufficiently heated, the fuel begins to pyrolyze and release flammable gasses. Once the concentration of these gasses reaches a critical lower flammability limit (LFL), flaming ignition occurs above the surface of the fuel [17]. Flaming ignition can occur in either a piloted, where a flame or hot source is nearby, or un-piloted mode, with the former resulting in easier ignition. Flaming combustion typically occurs when higher levels of heat flux heat a fuel to an ignition temperature rapidly or following smoldering ignition of a fuel, where a smoldering front progresses through a material initiating some pyrolysis as well, which ultimately forms enough flammable gases above the fuel surface so that ignition can occur. This process, the transition to flaming, is incredibly stochastic and remains a somewhat unsolved problem in the field [18, 19, 20, 21]. In other words, if conditions change such that heat transferring from firebrands to the fuel bed increases to the level of a critical flaming heat flux, a flame starts to appear above the fuel surface. Many studies have been performed investigating how firebrand can ignite different materials in both smoldering and flaming conditions. However, most previous research has focused on vegetative fuel beds.

2.3. Ignition of Vegetative Fuels

Hadden et al. studied the ignition of fuel beds by hot particles. In that research, spherical steel particles with different diameters and initial temperatures were individually dropped over a cellulose fuel bed and the ignition propensity was determined. Hadden's study incorporated a hot-spot ignition theory that helped to qualitatively describe the hyperbolic relationship between particle diameter and initial temperature of the particle, shown in Figure 2.2. Regimes of flaming, smoldering, and no ignition were delineated under various conditions. Later studies by the same group extended this work under more wind speeds and with different materials [22, 23, 24, 25, 26].

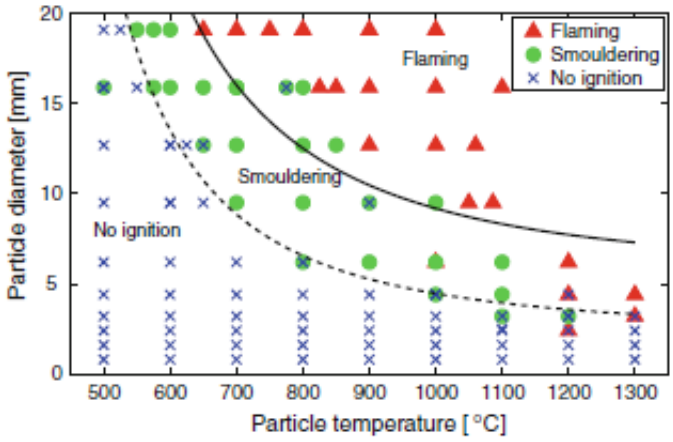

Figure 2.2: Ignition propensity of dry cellulose using heated steel spheres. This figure shows the quality of ignition depend on particle size and temperature [1]

Wang et al. continued studying hot particle ignition of vegetative fuel beds incorporating varying moisture contents [27]. Firebrands were modeled as steel spheres with diameters of 6, 8, 10, 12 and 14 mm and initial temperatures of 600-1200°C. Pine needles with different moisture content (MC) levels were used as the fuel bed. Effects of the temperature of the particles, fuel MC, wind speed, and particle diameter on the time to flaming ignition of the fuel beds were determined. A heat transfer analysis was proposed to indicate the parameters controlling the time to flaming ignition for different conditions. Yin et al. also studied the effect of MC on fuel bed ignition [28], finding a nearly linear correlation between MC and ignition propensity.

Manzello et al. [29, 30] has studied ignition of vegetative fuel beds on flat surfaces as well as of dense fuel beds in a crevice geometry using single and multiple cylindrical firebrands. Ignition conditions are presented of different materials under different conditions. It was concluded that even a single brand can ignite loose, vegetative fuels near a structure, however multiple firebrands are necessary to ignite fuels as they become denser.

Viegas et al. [31] studied the ability of bark and pine cones to ignite eucalyptus leaves, pine needles, hay, and straw. The fuels were studied under both live (moist) and dried conditions. Without wind, it was found that smoldering firebrands had a difficult time igniting fuels, however ignition was sometimes achieved with flaming

firebrands. Ellis [32] also performed ignition experiments over eucalyptus fuel beds. The moisture content of fuel was varied between 4-21 percent and wind speeds of 0-2 m/s were applied during the tests. Higher wind speeds were required to ignite fuel beds with higher MC levels.

Warey developed a model to determine the effect of thermal contact on the heat transfer between a glowing firebrand and fuel beds [33]. In this research, firebrands considered as two shapes of cylindrical and disk firebrand and a model was proposed to estimate thermal contact resistance between single firebrand and fuel beds. The disk firebrands were produced from douglas fir with diameter of 50 mm and thickness of 6 mm with initial mass of 6.3 g. Also douglas fir was used to produce cylindrical firebrand with diameter of 10 mm and height of 70 mm. This model is able to study the response temperature of fuel bed in different depths when a single glowing firebrand is deposited over the fuel bed with different relative contact pressure between firebrand and fuel bed. Also the ambient temperature, wind speed and fuel properties was assumed constant for all modelings. Higher peak temperature was observed with larger relative pressure and temperature on fuel bed with low microhardness was found be higher when glowing firebrand is deposited over them.

2.4. Ignition of Dense Fuels

Waterman and Takata [34] were among the first to study ignition of structural fuels by firebrands, using various roofing materials to simulate firebrands. Numerous later studies by Manzello and Suzuki have investigated the propensity for ignition of specific building assemblies using a firebrand generator, the "NIST Dragon" within a wind tunnel [35, 36, 37, 38, 39]. Several of these studies that are relevant to this work be reviewed, however this list is not comprehensive.

Suzuki et al. studied ignition of wood fencing assemblies by firebrand showers produced by the NIST firebrand generator (Dragon) in a wind tunnel with a constant 8 m/s wind speed [2]. The fencing was observed to achieve ignition under some conditions, however dried mulch beds below the fences, simulating real fuels, resulted in much easier ignition [2].

Figure 2.3: Flaming in the corner assemblies were additional fuel was presented. Also firebrand generated from fences can be seen. (From [2]

Studies by Manzello and Suzuki [40] presented that wind driven firebrands can form a pile over dense fuels such decks an ignite them. In this study, firebrands are generated in NIST firebrand generator and three type of fuels were exposed to firebrand shower with speed of of 6 m/s. Fuel density and moisture content were found to affect time to ignition of the fuels in their experiments.

Manzello et al. [12] also studied the ignition of plywood and OSB in crevice geometries. Firebrands were deposited over crevices with angle of 60° to 130° and time to ignition and net heat flux were calculated from results. It was found at wind speed of 2.4 m/s, critical ignition angle stands between 90° and 135°. These results clearly demonstrate that firebrands are able to ignite common building materials.

In other studies, Hakes et al. [14] studied the role of a firebrand's diameter and the size of a firebrand pile to heating and ignition of a solid fuel. Although pile size (mass) was found to be an important factor increasing the heat flux from firebrands to a fuel surface, the diameter of cylindrical firebrands made from the same material (birch) had a limited effect on measured heat fluxes. The importance of wind speed was also highlighted, with dramatically larger heat fluxes found for for the ignition of a fuel bed was determined which in this case, it was observed that ignition may only happen when wind is presented. In this research Oriented Strand Boards were used as fuel beds and firebrands were deposited over fuel bed in piles

with different mass. It was found that firebrands cannot ignite fuel beds in flaming condition when there is no wind. Also a methodology was found to determine heat flux from glowing firebrands both in single-point measurements by water-cooled heat flux gauge and spatial measurements by thinskin calorimeters. Water-cooled gauges may have cooling effect on firebrands. In order to avoid this cooling effect, gauges with relatively small diameter (in this case 1.27 cm) should be used.

Chapter 3: Experimental Methods

3.1. Overview of Experiments

Experiments presented in this study used two different apparatus in order to isolate the effects of heating from a pile of firebrands and interaction with a recipient fuel. Before either of these configurations were used, firebrands were generated from cylindrical wooden dowels and ignited in a smoldering mode. After production, brands were deposited either over a sensor array mounted on an inert ceramic base or directly over a recipient fuel. All experiments were preformed in a small-scale wind tunnel so that the pile size, brand properties, and ambient wind speed could be varied throughout experiments. The following sections describe the steps necessary to produce firebrands in this study, the wind tunnel and sensor array, and the procedure for both inert and ignition tests.

3.2. Firebrand Production

Cylindrical birch and oak wooden dowels with an initial diameter of 1.27 cm and a length of 2.54 cm were used to emulate firebrands from vegetative fuels. They were cut to length, dried, measured and weighed, revealing an oven-dry density of 520 to 580 kg/m^3 for birch dowels and a more uniform density of about 620 kg/m^3 for oak

dowels. Birch dowels were purchased from two different vendors to assess supplier variability. Several differences were noted in the experiments (e.g. different dry densities of firebrands which caused different resulting heating behavior). Dowels were placed on a perforated metal tray and placed within a laboratory oven at 104°C for drying, similar to ASTM D4442 [41]. During initial testing, dowel mass was monitored every 4 hours until changes in mass were negligible, indicating an oven-dry condition. Later tests involved at least 24 hours of drying before testing, as it was observed no measurable mass change was observed after that duration. After drying, dowels were stored in zip lock bags filled with a desiccant before being used in tests.

Before each test, the desired initial mass of firebrands was measured from dried dowels using a load cell with an accuracy of 0.1 grams. These dowels were deposited flat onto the center of a flat metal mesh basket which was placed over a propane burner until all dowels ignited. After achieving a uniform flaming ignition of all dowels (approximately 5–10 s after ignition of the burner), the burner was turned off to let the firebrands burn freely and reach a smoldering state of combustion. This process took about 10–15 s for the 50 g pile and about 30 s for the 100 g pile. The mass of dowels significantly decreased by this point, necessitating measurement of the deposited mass. The mass of smoldering firebrands was measured again with the

same load cell, depositing the smoldering brands onto a sheet of ceramic insulation board atop the load cell. These experiments were conducted separately from other experiments, with at least 10 repetitions to determine the average deposited masses for each test condition.

In both ignition and thermal measurement tests, smoldering firebrands were deposited over a sensor array or fuel bed using a funnel-like dumper with an outlet area of 10 cm $\times$ 10 cm (shown in Figure 3.1). This yielded a contact area between firebrands and fuel beds that was relatively uniform (10 cm x 10 cm) in all experiments.

3.3. Wind Tunnel

Experiments were performed in a small, enclosed wind tunnel which was able to generate ambient wind conditions in the range of 0.5 m/s to 3.5 m/s, shown in Figure 3.1. A 30 cm $\times$ 30 cm inlet reduces into a 25 cm $\times$ 7.5 cm test section made of stainless steel and is exhausted through a variable-speed high-temperature fan. The interior of the setup is painted with matte black paint to reduce re-radiation from wind tunnel walls and a 20 cm $\times$ 6 cm window of borosilicate glass is used to provide virtual access to the experiments. A 15 cm $\times$ 12 cm hole provided at the bottom of the wind tunnel allowed for either a sensor array or fuel sample to be inserted for testing. An additional small hole, 1.5 cm in diameter just past the reducing section

allows for a hot-wire anemometer to be inserted at different heights, measuring the ambient wind speed. Wind speeds were found to have a somewhat flat profile with height, although calibrated corrections were applied because a blockage of firebrands is essentially placed within the tunnel (see section 3.6.3). This correction becomes significant when wind speeds are larger than 2 m/s, above the majority of tested conditions.

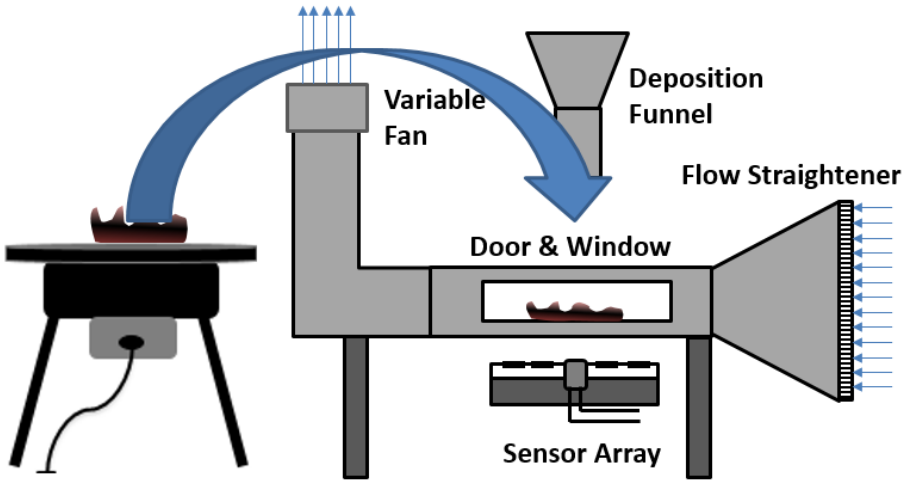

Figure 3.1: Schematic of the experimental setup showing a wind tunnel, sensor array, and burner in a side view.

3.4. Thermal Sensor Array

Three types of sensors were used for thermal measurements over a 1.27 cm thick sheet of Superwool 607 High temperature ceramic insulation board, which simulated a relatively adiabatic surface. First, a 1.27 cm diameter Medtherm (GTW-7-

32485A) water-cooled heat flux gauge (WC-HFG) was used to precisely measure the time-resolved heat flux at the center of the array. Unlike individual brands whose heating is dominated by conduction and surface contact, in piles it is thought that re-radiation plays a significant role in heating, justifying the use of radiation-based gauges. To provide a spatial representation of heat flux and temperature, 16 thin-skin calorimeters (TSC), consisting of thin sheets of metal with a K-type thermocouple spot welded to their rear surface, were installed over the 10 cm $\times$ 10 cm region, shown in Figure 3.2. To directly measure temperatures closer to the surface of firebrands, five fine-wire (30 gauge) K-type thermocouples were placed adjacent to 5 TSCs, providing relative measurements of glowing firebrand temperatures. These were not secured in any way, but instead held down by weight of the pile.

TSCs consisted of a 30 gauge Chromel-Alumel K-Type thermocouple welded to the back of a 1 cm $\times$ 1 cm $\times$ 0.1 cm Inconel alloy 625 plate. The top surface of the TSC was painted matte black using high temperature Zynolyte paint. Some changes in the color of sensors were observed after repeated tests, so sensors were cleaned and re-painted every 5-10 tests depending on the condition of the paint. TSCs were spaced around a central WC-HFG in two rows, later referenced as "inner and outer" TSCs, shown in Figure 3.2. While the design of TSCs was intended to provide relative heat flux readings following ASTM E459 [42] and Hidalgo et al. [43], it was later

found that errors in calibration were too great to provide reliable heat flux readings. TSCs did, however, provide reliable temperature readings akin to what would be observed on the surface above the inert material, and were interpreted throughout the tests as such.

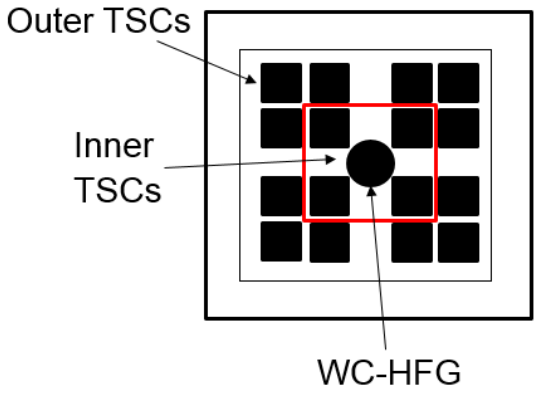

Figure 3.2: Schematic showing sensor WC-HFG and TSC locations over an inert board. Four inner TSCs and 12 outer TSCs are indicated, later used to distinguish temperatures near the center and edge of firebrand piles.

3.5. Ignition Tests

All experiments for inert arrays were repeated under the same conditions (wind speed and mass of deposited firebrands) over fuel samples. Fuels were chosen from common wooden structural materials, plywood and lumber, with relatively different densities. Fuel samples were cut to the dimensions of 15 cm $\times$ 15 cm and a thickness of 1-2 cm. All samples were fully dried in a convective laboratory oven with a temperature of 104°C until there was no change in mass, at least 3 hours. Five holes

were drilled along the center-line of the samples, terminating 0.5 cm from the surface. Five 30 gauge K-type thermocouples were pinned to these holes resting 0.5 cm from the surface, shown in Figure 3.3. These temperatures were used to determine the time to smoldering, noting when the smoldering front progressed in depth and along samples. All test were also recorded with a Sony Handycam HD camcorder through a side-view window in order to observe the onset of flaming. All tests were allowed to continue until flames appeared over the fuel surface or the smoldering front reached the bottom of the fuel sample.

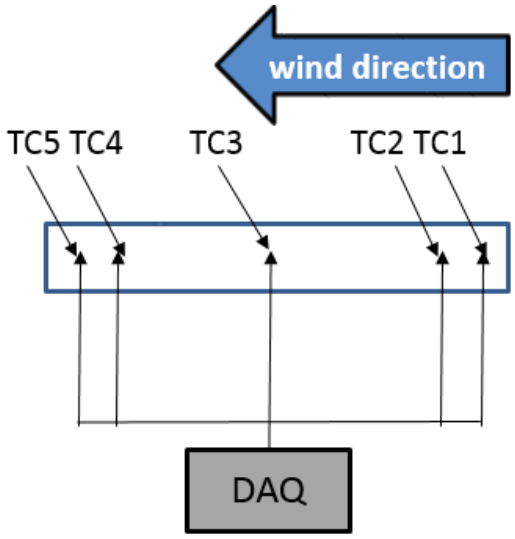

Figure 3.3: Schematic showing a side-view of a wooden sample used during igntition tests. Thermocouples are labeled TC1 to TC5.

Measured thermocouple temperatures were used to determine the onset of smoldering within fuel samples. Due to the constantly changing shape and structure of

different fuels as they smolder, it was difficult to interpret measured temperatures as the TCs physically moved during the tests. To overcome this challenge, several different fuels were burnt at different conditions for different lengths of time, extinguished, and cut along the centerline to observe the depth of char progression. ImageJ was used to manually select the outer extents of the char fronts from images of cut samples and connect them with TC locations. An example of such an image is shown in Figure 3.4. Comparing these images to TC measurements, a common threshold of 200°C was found, with the smoldering front reliably reaching the TC displaying 200°C. While this value is below what would typically be considered the onset of smoldering, it empirically best-represented the behavior visually observed in tests. As smoldering progressed over a relatively short distance, a threshold of 200°C was set for the TC directly below the center of pile to represent smoldering ignition.

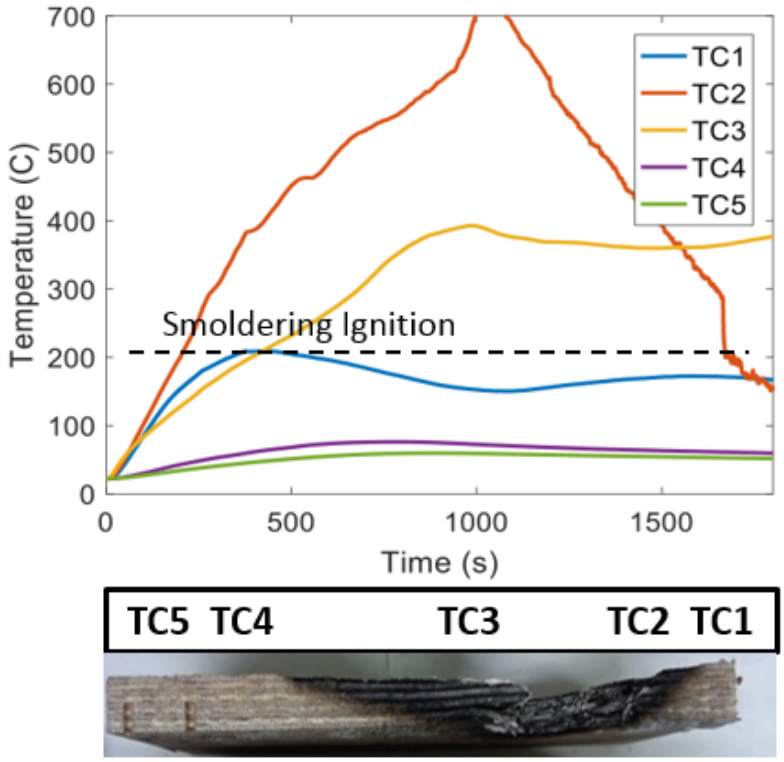

Figure 3.4: The top figure shows TC measurements at 5 locations along the centerline of a plywood fuel sample. The bottom figure shows a corresponding side-view photograph of the centerline o the cut sample used to determine threshold for smoldering ignition. Two holes for thermocoupels on the left-hand side are still visible, while the others have deformed and are no longer visible.

3.6. Calibration

3.6.1. Water-Cooled Heat Flux Gauge

In initial testing the WC-HFG used in these experiments was calibrated under a standard cone calorimeter [44] against a NIST-traceable heat flux gauge. Due to degradation of the sensor surface and paint during testing, a radiant propane heater

was also used to calibrate the surface of the sensor against the same gauge every 10–30 tests, depending on the level of degradation seen. Occasional cleaning and re-painting of the sensor surface with Medtherm branded paint was also occasionally conducted, followed by re-calibration. This calibration methodology was acceptable as a majority of heat transfer from firebrands to sensors was assumed to occur via radiation.

Calibrations using a propane radiant heater consisted of placing the WC-HFG 1 mm apart from a calibrated 2.54 cm WC-HFG in the same plane at the same distance from the edge of the propane heater. Care was taken that both gauges remained outside of the convective boundary layer and were moved backwards from this closest distance over a range of heat fluxes. A calibration coefficient was then recorded for the WC-HFG between voltage and heat flux, comparing against values from the calibrated gauge. Following a maximum heat flux of about 40 kW/m^2, the error in calibration was about 5%, well within the range of repeatablity for these experiments. While some heat fluxes did rise above this level, it is not expected the gauge would become nonlinear between cone-calorimeter calibrations which could be performed at higher heat fluxes and these higher heat fluxes did not last for an appreciable amount of time.

3.6.2. Thinskin Calorimeters

TSCs were initially designed for this study in order to collect a spatial map of heat fluxes from firebrands. Previous work by Hakes et al. [14] has shown this technique to be feasible using a calibration methodology by Hidalgo [43]. However, this was performed without external wind. When an external wind is applied, which is required in order to achieve ignition of fuel samples, the influence of convective cooling on the sensor starts to dominate the process. This component is difficult to estimate, as the pile of firebrands provide a large blockage and conditions are unknown underneath the pile, where most sensors are located. Therefore, errors become too high to use for these tests. It was suspected, however, that direct temperature measurements may still be useful when spatially applied over the surface.

Four K-type thermocouples were used during inert tests to verify the temperature measured by TSCs was similar to firebrand surface temperatures measured. Five tests were performed for a 0.5 and 0.8 m/s wind speed with 16 g of smoldering firebrands deposited over sensors. Those five thermocouples were placed so that they were in-touch with a firebrand and each was placed exactly on top of one TSC at the start of each test. Figures 3.5 and 3.6 show a comparison between TSC temperatures and adjacent TCs. As can be seen in Figures 3.5 and 3.6, TSC temperatures match relatively well with thermocouple measurements. The mean temperature between 5

sensors are averaged between 5 repeated tests to form the solid lines in both figures, revealing a close trend, although the TSCs reach a slightly lower peak temperature at lower wind speeds. With the wide variability present in these sort of experiments, TSCs are seen to provide a useful measure of temperatures over an inert surface without the wide variability and constant breakage of fine thermocouples seen in repeated tests.

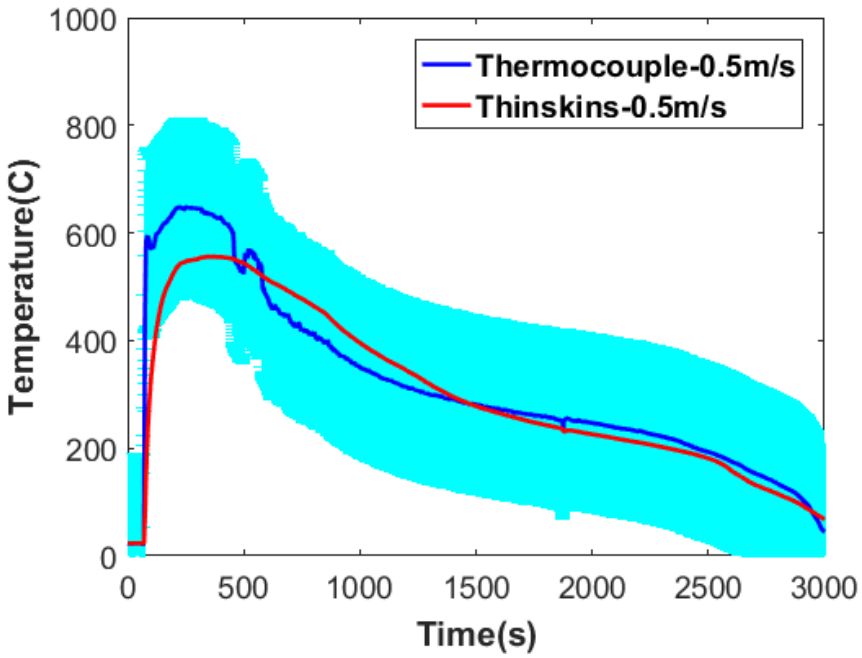

Figure 3.5: Temperatures from TCs and TSCs with 16 g of firebrands deposited over a sensor array under a wind speed of 0.5 m/s. Each solid line represents temperatures from TSCs or TCs averaged between 5 repeated tests over 5 locations. The shaded area represents the standard deviation between the tests and locations, with TSCs having slightly less variability.

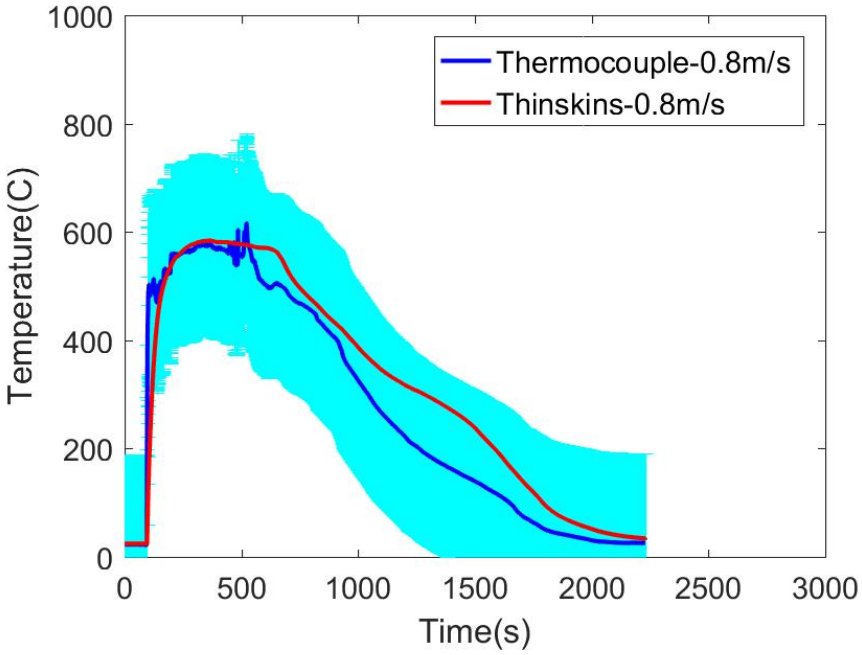

Figure 3.6: Temperatures from TCs and TSCs with 16 g of firebrands deposited over a sensor array under a wind speed of 0.8 m/s. Each solid line represents temperatures from TSCs or TCs averaged between 5 repeated tests over 5 locations. The shaded area represents the standard deviation between the tests and locations, with TSCs having slightly less variability.

It is also important to investigate the surface temperature of firebrands, in particular as they contact a simulated fuel surface below a pile. As mentioned above, 4 K-type thermocouple were used to measure the surface temperature of firebrands, placed directly below the pile and above a TSC near the center. Temperatures from these 4 thermocouples are presented in Figures 3.7 and 3.8. These temperatures clearly show some variability due to many effects, such as movement over time as firebrands degrade, blowing by wind, etc., however they still reflect the surface tem-

perature of firebrands between the pile and inert surface.

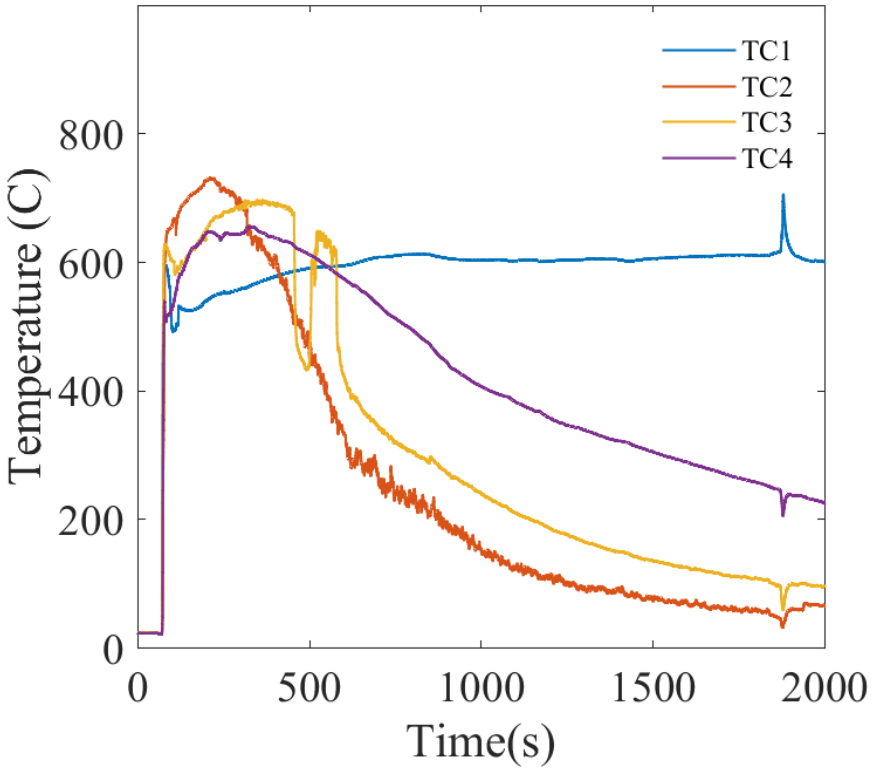

Figure 3.7: Temperatures from TCs with 16 g of firebrands deposited over a sensor array under a wind speed of 0.5 m/s.

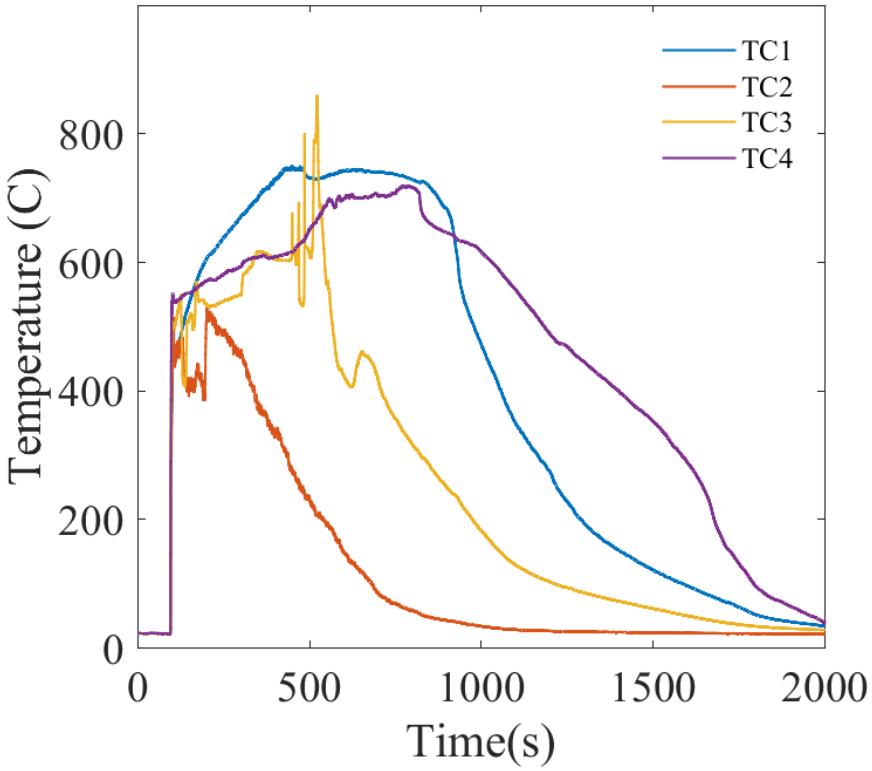

Figure 3.8: Temperatures from TCs with 16 g of firebrands deposited over a sensor array under a wind speed of 0.8 m/s.

3.6.3. Wind Speed

Wind was generated for these tests using a variable-speed fan to generate a flow within a wind tunnel which had a honeycomb and converging region upstream. The wind speed was measured using a 6006 Kanomax Hotwire Anemometer LITE. A small hole was made in the wind tunnel along the bottom plate a few centimeters before the test section such that the hotwire anemometer could be inserted from the

bottom of the wind tunnel and pushed up to different heights above the surface. Because the fan was used on the outlet in a suction mode, the presence of a pile of firebrands had an effect on the wind speed. To compensate for this, measurements were made with and without an obstruction. This obstruction was made from 100 g of dried birch dowels with a 1.27 cm diameter, modeling the presence of a common 16 g pile of smoldering firebrands. Resulting measurements with and without an obstruction are shown in Figure 3.9. Measurements could only be made from 25-55 mm above the surface of the wind tunnel due to the geometry of the sampling port.

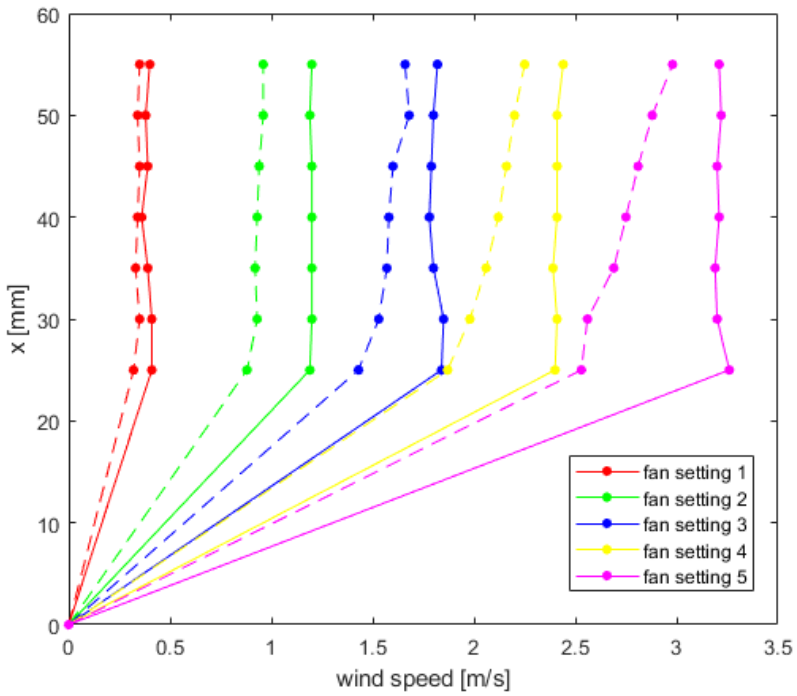

Figure 3.9: Wind speeds measured at different heights above the surface of the wind tunnel with an average wind speed from 0.5 m/s to 3.5 m/s. The solid lines show the wind profiles measured before depositing firebrands and dashed lines show wind profile with firebrands deposited.

As the wind speed increases, the presence of an obstruction, i.e. firebrands, becomes significant and this effect needs to be considered when reporting the wind speed tests are conducted at, especially when the wind speed is higher than 1 m/s. A calibration using this reduction is applied to all further results, graphs and calculations. At the highest wind speeds, higher than 3 m/s, the wind profile in the presence of firebrands is no longer uniform, so no tests have been conducted at these wind speeds.

Figure 3.10: Photographs showing the methodology used to measure wind speeds including the tip of the hot-wire anemometer (right) and wind speed measurements being performed with a simulated presence of firebrands (left).

Chapter 4: Results

4.1. Summary

Results are presented first for inert tests using a sensor array and later with representative fuels to investigate ignition of solid fuels by piles of firebrands. Data extracted from both series of tests, i.e. heat fluxes and temperatures from the inert tests and time to smoldering or flaming ignition in the material tests were compared to shed light on the phenomena leading to ignition of different materials.

4.2. Time-resolved Heat Flux

Time-resolved single-point heat flux measurements were performed using a water-cooled heat flux gauge (WC-HFG) inserted into the center of an inert sample, described in Chapter 3. The water-cooled gauge provides a calibrated, time-resolved heat flux at a single point during experiments, shown in Figure 4.1. Experiments were performed under a variety of firebrand loading conditions (e.g. deposited pile mass) and ambient wind speeds. Figure 4.1 shows the result of these tests performed with 16 g of smoldering birch dowels deposited on the inert sensor array for wind speeds of 0.5, 0.8, 1.2 and 1.4 m/s.

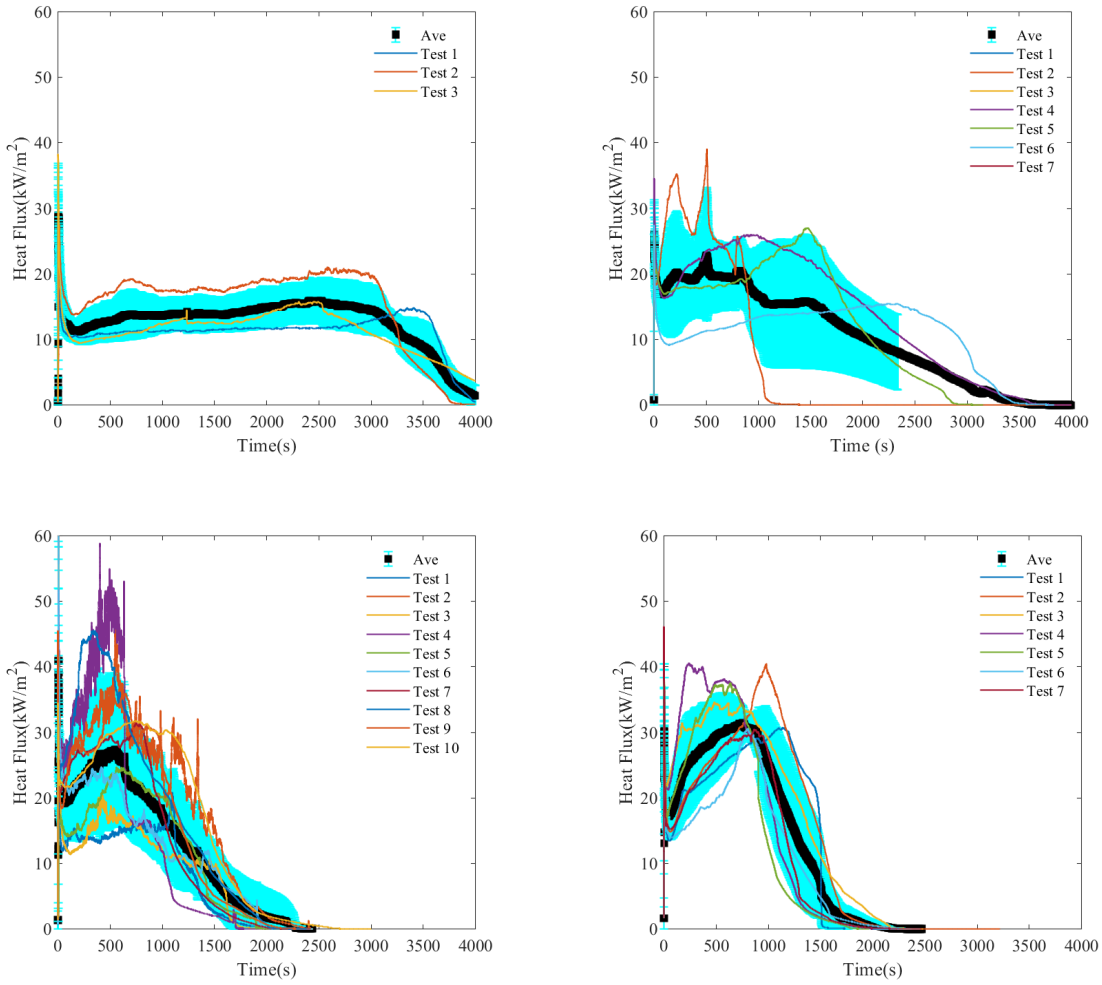

Figure 4.1: Heat fluxes recorded from a WC-HFG are shown with 16 g of smoldering birch firebrands deposited over the sensor under different wind speeds. The shaded area represents a standard deviation between tests. Note the birch used was from vendor 1.The wind speed is 0.5 m/s in the top-left graph, 0.8 m/s in the top-right graph, 1.2 m/s in the bottom-left graph and 1.4 in bottom-right graph.

In figure 4.1 it is clear that the wind speed has a considerable effect on both the heating duration and the peak heat flux for the same firebrand pile size. Higher wind speeds are shown to yield a higher peak heat flux but also result in a shorter

heating duration. This is, perhaps, to be expected, as higher wind speeds are later shown to produce higher temperatures as a result of increased surface oxidation, which would invariably increase heat fluxes to the surface. As heat is released at a higher rate, firebrands burn out faster, resulting in a reduced duration of heating. While increased wind speeds may increase the cooling rate from firebrands, it appears that the effect of increased rates of oxidation is considerably larger than any cooling effects within the regimes tested here.

The number of tests performed at each condition was determined based on the variability of heat flux measurements from test to test. Thin lines in Figure 4.1 represent individual tests while the thick black line represents a mean between all tests. For example, in conditions which had fairly repeatable behaviors (i.e. 0.5 m/s), only three tests were performed. At 1.4 m/s, which lies at a transition point between smoldering and flaming, results were seen to be quite variable. Here, 10 tests were performed in order to calculate a more reliable average for that condition. It follows that the standard deviation between tests, shown in a light blue shading in Figure 4.1, increases as the variability of tests increases, even when tests are repeated up to 10 times (0.8 and 1.4 m/s). This is not necessarily due to errors in the measurement techniques, which show clear trends for tests at 0.5 m/s. Instead, it is indicative of the stochastic nature of transition between flaming and smoldering,

as in some experiments the pile would transition to flaming, and others it would not, dramatically affecting the heat fluxes measured.

Even for experiments over an inert substrate, piles of firebrands sometimes transition to flaming under high enough wind speeds. The probability of transition to flaming is determined from recorded the videos of experiments for each wind speed and deposited mass conditions. Figure 4.2 shows this probability that flames are observed in a test, determined from the overall number of tests performed and how many have ignition observed in each condition.

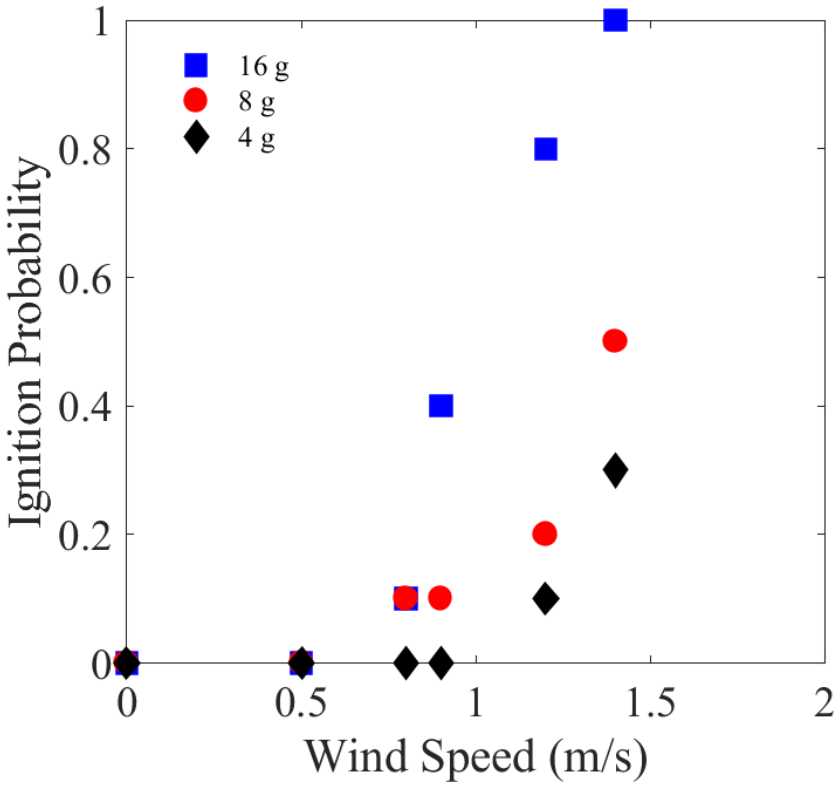

Figure 4.2: The probability of flame appearance over smoldering firebrands during experiments over an inert substrate.

According to these probabilities, transition from smoldering to flaming over firebrand piles (defined as where this probability reached 0.5) occurs at around 1.2 m/s for 16 g and 1.4 m/s for 8 g initial deposited mass piles. This is responsible for some of the variability in heat flux results shown in figures 4.1 and 4.3 for wind speeds of 1.2 and 1.4 m/s. Also, figure 4.2 shows the fact that the probability of transition from smoldering to flaming is very low when 4 g of firebrands are deposited over a

fuel, with less variable heat flux results shown in figure 4.4.

The mass of deposited smoldering brands also affects the level of heating received to an inert surface. Figures 4.3 and 4.4 show experiments performed under the same wind speeds as Figure 4.1, but instead with 8 and 4 grams of deposited firebrands, respectively. As expected, heat fluxes are reduced as the mass of the firebrand pile deposited reduces, however, less reduction is seen between 16 to 8 g vs. 8 to 4 g. As will be shown later, it appears the peak heat flux starts to plateau after a critical pile size, but does increase up to that point with increasing mass.

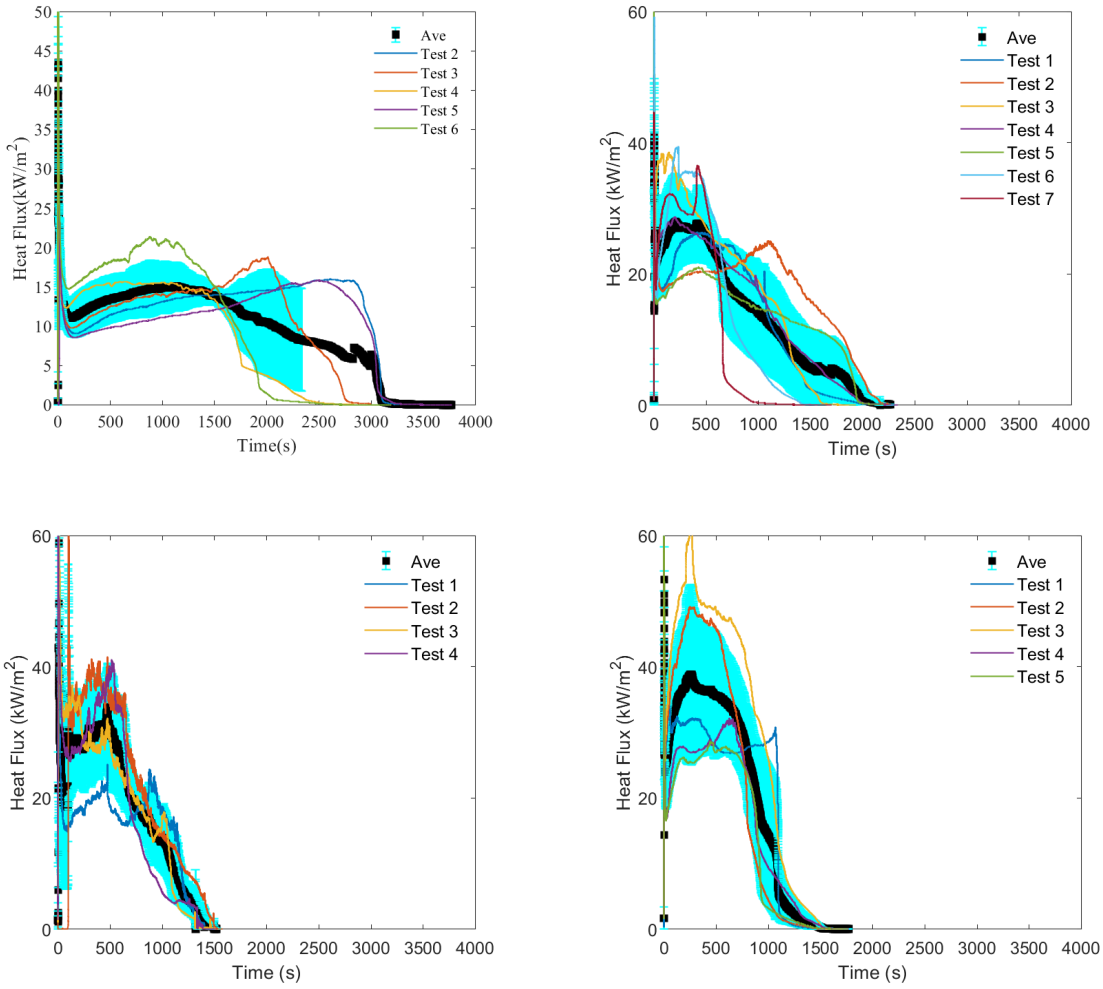

Figure 4.3: The heat flux from WC-HFG data when 8 g smoldering birch firebrands were deposited over sensors in different wind speeds. Shaded area shows standard deviation for all tests have been done which birch from vendor 1. The wind speed is 0.5 m/s in the top-left graph, 0.8 m/s in the top-right graph, 1.2 m/s in the bottom-left graph and 1.4 in bottom-right graph..

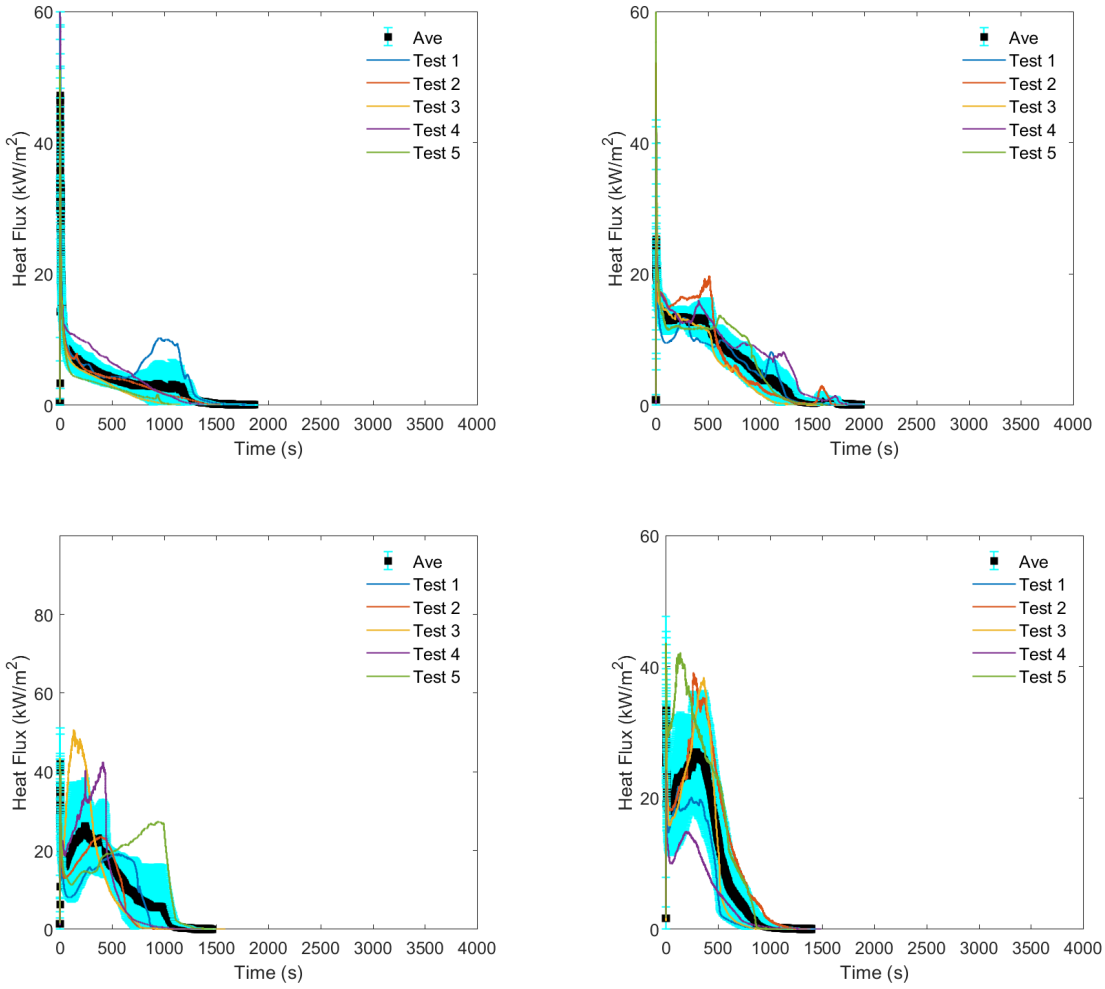

Figure 4.4: The heat flux from a WC-HFG when 4 g of smoldering birch firebrands were deposited over sensors in different wind speeds. The shaded area shows the standard deviation for all tests. The wind speed is 0.5 m/s in the top-left graph, 0.8 m/s in the top-right graph, 1.2 m/s in the bottom-left graph and 1.4 in bottom-right graph. Note the firebrands are made of birch wood from vendor 1.

Heat fluxes averaged at each time step for different wind speeds and initial masses were re-plotted in Figure 4.4 to show the effect of wind speed on heat flux for each pile size. It is clear that, as the mass of the pile increases between 4 to 8 g, there is a

large uptick in the peak heat flux; however, there is little difference between 8 to 16 g, except that the duration of heating generally lasts longer. An effect ignored here is the area that receives this heat flux. A larger pile will presumably heat a larger area, which will be discussed later when TSC measurements are presented.

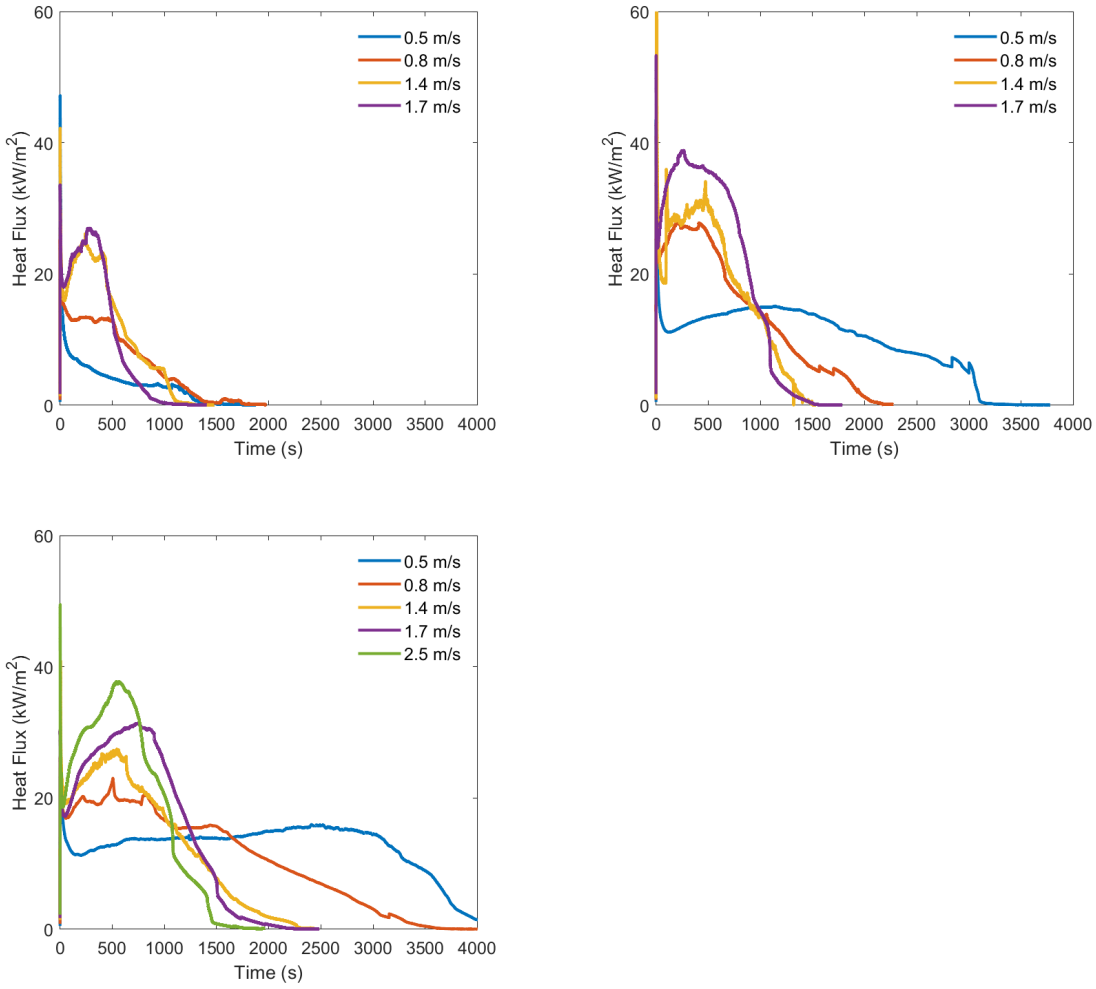

Figure 4.5: The average heat flux from a WC-HFG when 4, 8 and 16 g of smoldering birch firebrands were deposited over inert sensors under different wind speeds. The deposited mass starts at 4 g in the top-left graph, 8 g in the top-right graph and 16 g in the bottom-right.

Interpretation of time-varying heat flux measurements and their comparison for different firebrand loading and ambient wind speeds is complex. The peak heat flux obtained during a test is a simple quantity of interest which represents the magnitude of the maximum heat flux for each test condition. The peak heat flux derived from each averaged heat flux curve for a particular condition is plotted for different wind speeds in Figure 4.6. It was found that the peak heat flux is only dependant on the wind speed, with the effect of the deposited mass being negligible for a single type of firebrand used (in this case cylindrical samples of birch wood). A correlation between peak heat flux and wind speed,

$$q''_p = 15.9U_\infty + 9.18 \tag{1}$$

with $R^2 = 0.813$ is presented as a dashed line in Figure 4.6. In this correlation q''_p is the peak heat flux [kW/m^2] and U_∞ is the wind speed [m/s]. The slope of the relationship between wind speed and heat flux, C, is used in a scaling analysis in Chapter 5 as C. It should be noted this correlation should not be interpreted as being applicable to other configurations than the one presented in this study and is only a first approximation to investigate the effect of wind speed on peak heat fluxes from firebrand piles.

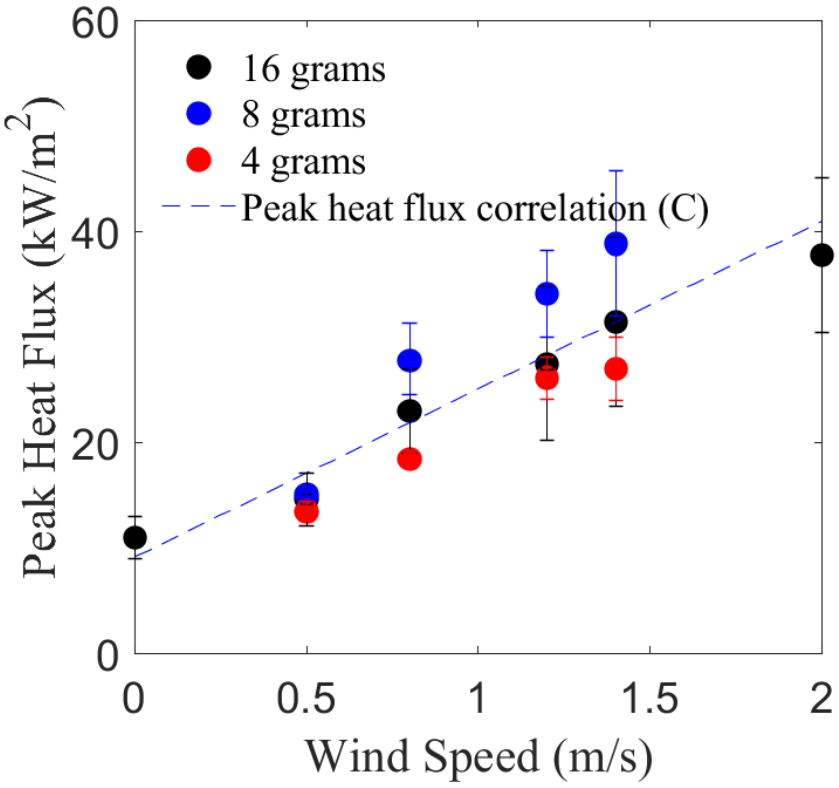

Figure 4.6: Peak heat fluxes from a WC-HFG for different firebrand mass loading and wind speeds. The error bars represent the standard deviation between the peak heat flux measured from different tests at each condition. The value of wind speed in this graph is corrected based on the wind speed calibration presented in the previous chapter. Data has been added to this figure from additional tests performed under no wind and at 2 m/s for 16 g of deposited mass to extend the range of measurements.

Up to this point all firebrands studied were fully-dried birch wooden dowels from one single vendor. In reality, firebrands may be generated from a wide range of materials, therefore it is important to determine what differences may result from various material properties. In order to study this effect, birch wood was purchased from another vendor, testing both variations in properties and differences in a single

wood sample, and oak wood samples from a single vendor. These samples were then also used to generate simulated firebrands in the same apparatus and combination of wind speeds and deposited mass. As with all previously-reported tests, all cylindrical dowels used here have an initial diameter of 1.27 cm and a length of 2.54 cm.

Initial testing of these wooden dowel samples found that there were major changes in their behavior compared to the original birch dowels from vendor 1. First, the density of each sample was determined. For each firebrand type, 10 random samples were chosen and their mass was measured with a load cell with an accuracy of 0.1 grams. All samples were fully dried before weighing. Then the dimensions of the firebrands were measured using calipers and densities were calculated. Densities presented are averages of measured densities for all samples. For each firebrand type, five tests following this procedure were repeated to generate a representative average of samples. These values and associated standard deviation of densities between repeated tests is shown in table 2.

Table 2: Firebrand Measured Densities $[kg/m^3]$			
Sample	Birch (Vendor 1)	Birch (Vendor 2)	Oak
1	517	600	651
2	518	581	652
3	541	585	643
4	529	591	623
5	512	571	671
6	560	561	639
7	519	595	651
8	520	602	641
9	549	605	642
10	509	601	639
average	527.4±16.16	589.2±13.84	645.2±11.75

In order to ensure consistency between tests, it was desired to keep the same deposited mass of smoldering firebrands at the start of all tests at the same condition, regardless of the original mass prior to ignition. Separate tests were run where various pile sizes were ignited and allowed to reduce to a smoldering pile, then deposited onto an inert board over a load cell rather than into the test section. At least 10 repetitions were conducted for each firebrand type. Results are presented in table 3. For

the original birch wood used, from vendor 1, the deposited mass was approximately 16 percent of the initial mass. However, birch wood from vendor 2 left only 10 percent of the original mass even under the same testing conditions. Then initial mass was therefore adjusted such that the deposited mass was constant for all wooden samples.

Table 3: Firebrand Measured Initial and Deposited Masses [g]

No	Birch(Vendor 1) -Initial Mass	Birch(Vendor 1) -Deposited Mass	Birch(Vendor 2) -Initial Mass	Birch(Vendor 2) -Deposited Mass
1	100	16.7	100	10.4
2	100	16.2	100	10.1
3	100	15.6	100	9.8
4	100	16.1	100	9.7
5	100	17.4	100	10.2
6	50	8.2	50	5.1
7	50	8.7	50	5.3
8	50	8.2	50	5
9	50	7.9	50	4.8
10	50	7.7	50	4.7

It is also important to determine the porosity of the deposited pile, in particular

if future efforts intend on modeling results of this study. In order to determine porosity, the bulk density of the deposited pile of firebrands was measured based on a deposited mass from measurements presented in table 3 and the bulk volume of pile measured from pictures of the experiments. Three tests for each deposited mass of 4, 8 and 16 g were chosen and pictures from a side and front view of the pile were analyzed with the software ImageJ. Figures 4.7, 4.8 and 4.9 show three side-view pictures of piles used to measure the bulk density of the pile. A ruler is used to scale to pixel readings from ImageJ and convert them to cm. The average height of the pile is used to measure the volume of the pile using the width and length of pile and assuming a cubical shape for each pile.

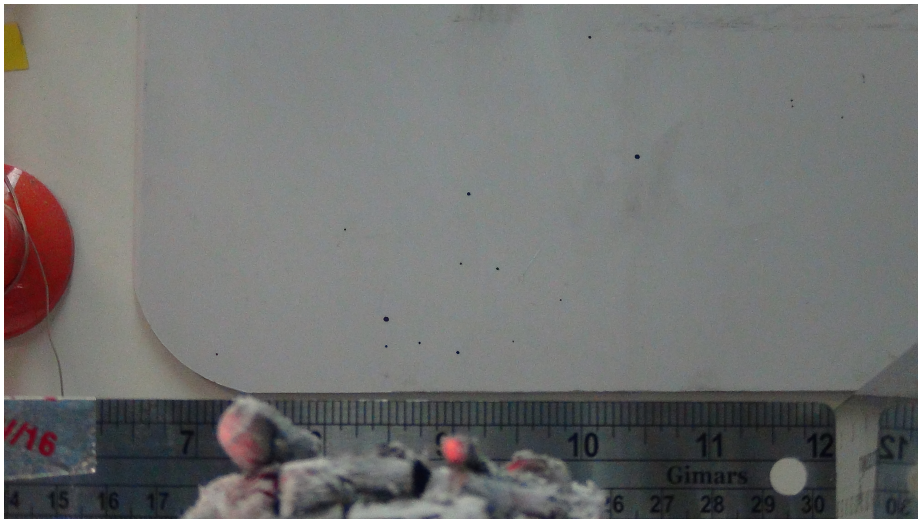

Figure 4.7: Side view photo from a pile with a deposited mass of 4g.

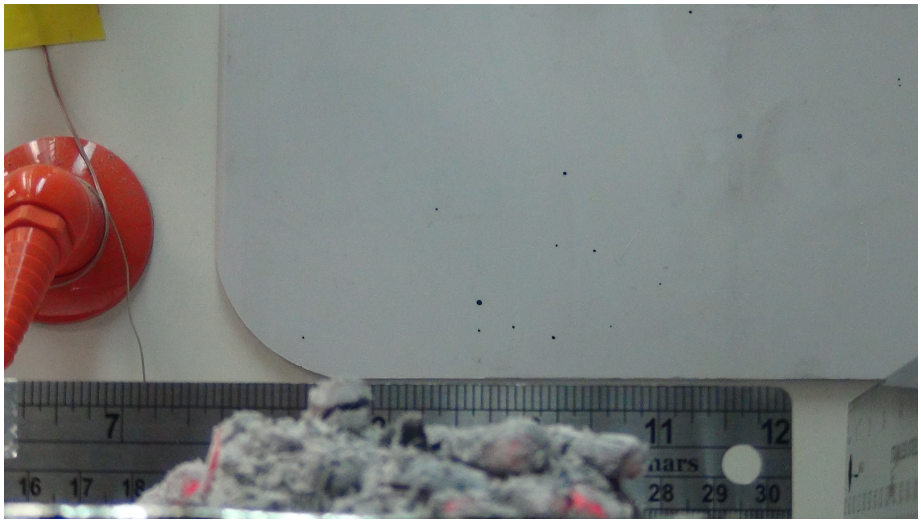

Figure 4.8: Side view photo from a pile with a deposited mass of 8g.

Figure 4.9: Side view photo from a pile with a deposited mass of 16g.

Figure 4.10 shows the bulk density of each pile for different deposited masses. Error bars are also shown to represent the standard deviation from 3 different tests performed to measure bulk density.

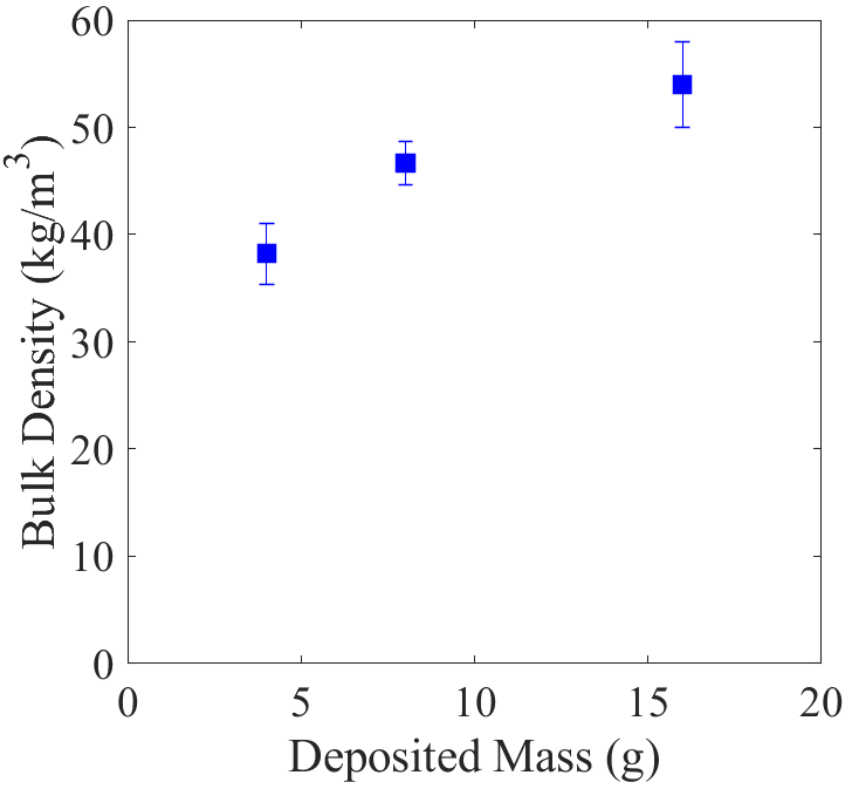

Figure 4.10: The bulk density of pile with respect to its deposited mass.

It is shown that by increasing the deposited mass of firebrands, the bulk density will increase or, in other words, the porosity of the pile deposited over the fuel is decreased.

Figure 4.11 shows the average heat flux recorded from experiments with birch wood from two vendors and oak wood, all with 8 grams of deposited mass over the sensor array under a wind speed of 0.5 m/s. Both the peak and duration of heat flux from these different brands vary considerably. Birch wood experiences relatively

similar trends from both vendors, however vendor 2 generally has a lower heat flux over the same duration. Oak dowels, however, reach a higher peak heat flux (∼20 kW/m^2 vs. ∼15 kW/m^2) but release heat over a shorter time, with slightly lower net energy release. Exactly how this relates to initial mass has yet to be determined, however this highlights the need to study different materials and ensure a uniform supply of wood for all experiments.

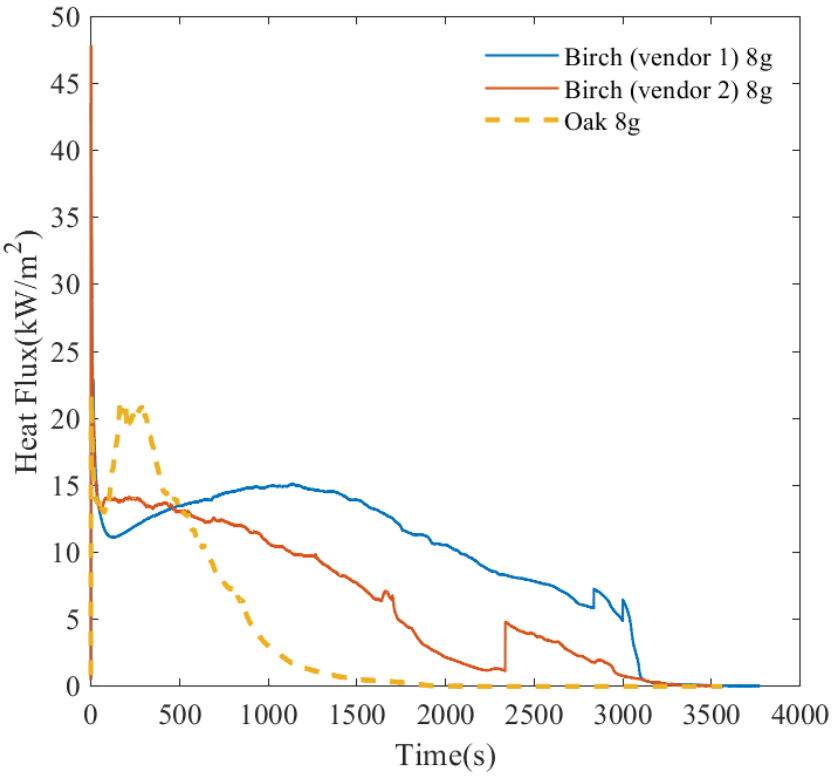

Figure 4.11: WC-HFG measurements of heat flux for 8 g of different firebrand types under a wind speed of 0.5 m/s. Heat fluxes shown are an average between at least 3 repeated tests.

Changes in the initial density and remaining mass after flaming point to dif-

ferences in the constituents within these samples, however this was not thoroughly investigated as part of this study. The initial density is one parameter that appears key as there was some variation in density between samples, and may help to describe some of the differences in the makeup of different wood species. This then relates to the ultimate heat flux observed. In the future, it would be of interest to study the chemical compounds in different wood samples and how that affects their smoldering and heating behavior.

To further demonstrate the effect of initial density, the peak heat flux from the three samples is plotted against density. Higher-density firebrands, at least for the limited set studied here, experience a higher peak for heat flux than similar piles under the same wind conditions.

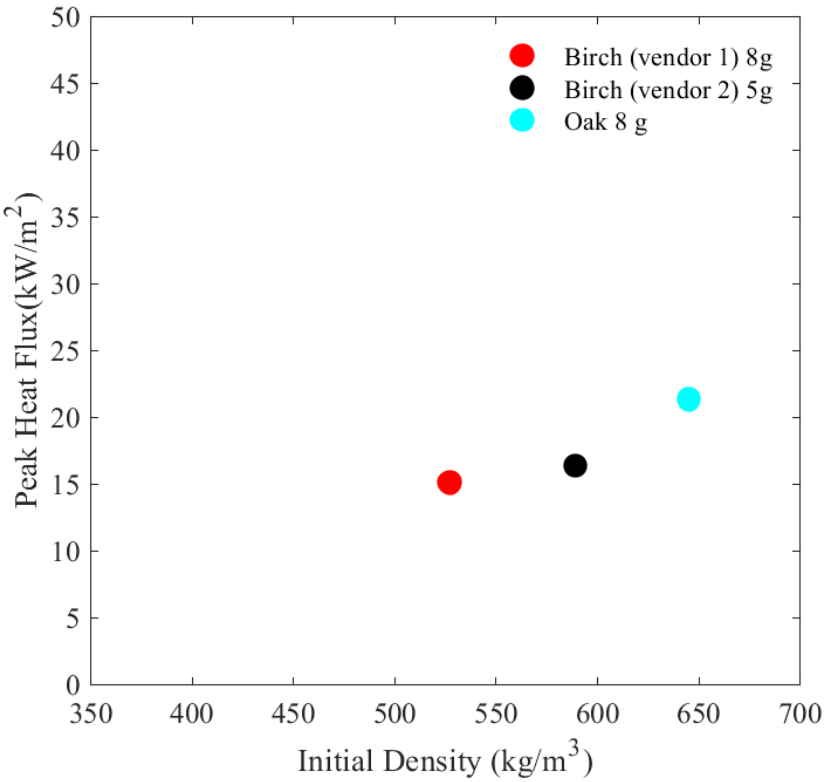

Figure 4.12: Peak heat fluxes extracted from WC-HFG measurements for an 8 g mass of firebrands from three different fuels deposited onto an inert sensor array under a 0.5 m/s wind. Peak heat fluxes were determined as the highest value over time along a curve averaged between repeated tests.

In a previous study by Hakes et al. [13] it was found that the size and shape of cylindrical firebrands (e.g. diameter and length) did not have a considerable effect on heating properties when all other factors remained constant. While the geometry of cylindrical brands does not seem to make much difference, it appears that the material used does make an important contribution that should be considered.

4.3. Total Thermal Energy Transport

As mentioned earlier, firebrand type, wind speed and deposited mass all the heating duration from firebrands. One way to consider this problem is to calculate the total thermal energy, E transported from firebrands to a fuel bed, over a net heating period, t. To do this, the area under heat flux curves, $\dot{q}''_f$ from Section 4.2 can be calculated,

$$E = \int_{t_1}^{t_2} \dot{q}''_f A_c dt \tag{2}$$

defining the total thermal energy transferred from firebrands to a fuel bed when the contact area, A_c remains constant. This is different than heat-release rate, which would be the net chemical energy released. Instead, we focus only on what heating could, when modeling this process over an inert surface, be transferred to the bottom boundary. Still, this should be related to the net energy content of the pile of firebrands.

This equation was used for birch dowels from vendor 1 on all conditions previously studied. E is plotted in Figure 4.13 as a function of wind speed. It is expected that the total energy released is dependant on the duration of heating from firebrands, which also corresponds to higher masses deposited. Interestingly, after reaching 8 g of deposited mass, little increase in net energy released is seen. This may be due to the

fact that there already is a sufficient hot pile covering sensors, but it is interesting as the burning duration does increase. Further study will be required to do a net energy balance and work out the components of heating to the fuel surface, i.e. conduction vs. radiation.

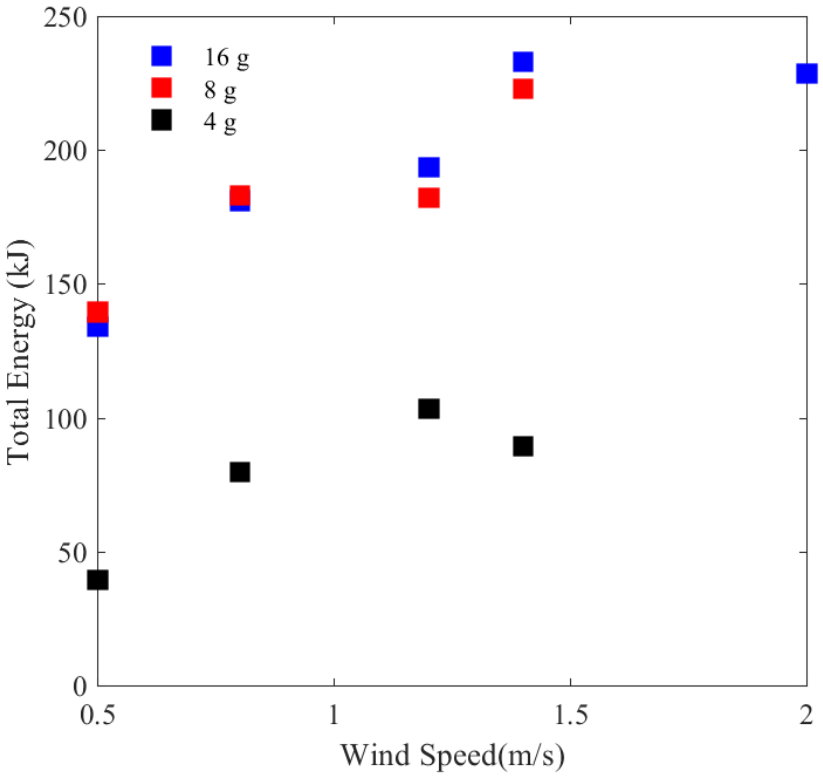

Figure 4.13: The total energy transferred from firebrands to an inert fuel bed is shown as a function of wind speed.

The total energy was also calculated for oak and birch dowels from two vendors following the previously-described approach. Figure 4.14 shows this effect for 8 g of deposited mass under a wind speed of 0.5 m/s versus the initial density of

firebrands. It was found that the total energy decreases when firebrands have a larger initial density. Whether this is due to more of the burnable components burning out during the ignition stage or another difference in the makeup of the fuel is currently unknown. Previous measurements in Figures 4.11 and 4.12 show that higher initial density firebrands have a somewhat higher peak heat flux, but this is compensated by a shorter heating duration.

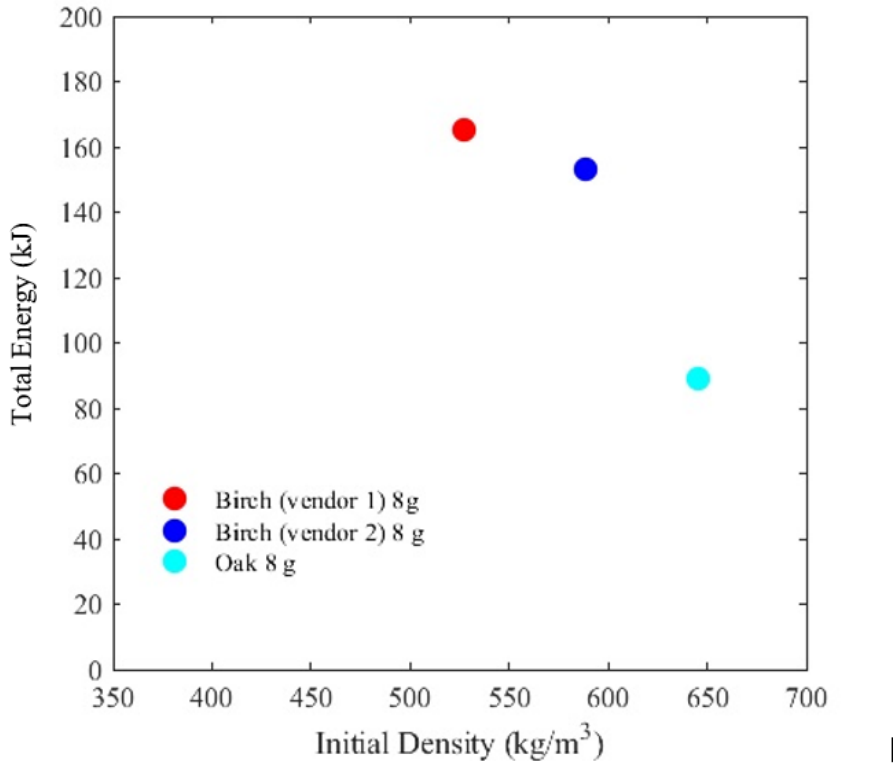

Figure 4.14: The total energy transferred from firebrands to an inert fuel bed is shown as a function of density for three fuel samples. All tests had 8 g of firebrands deposited over sensors under a wind speed of 0.5 m/s

4.4. Temperature Measurements

Thin-skin calorimeter (TSC) temperature measurements were conducted for all tests and presented in two ways. First, averaged temperatures of the inner group of four TSCs (TSC1) and outer 12 TSCs (TSC2) were presented for different experiments on birch dowels from vendor 1. The location of these sensors was shown previously in Figure 3.2. The inner TSCs (TSC1) therefore presents a representative temperature at center of the pile, close to the WC-HFG, while the outer (TSC2) sensors represent the temperature at the outer extend of the pile. A spatial view of temperatures is also able to be formulated for the 16 sensors used, presented later.

Figure 4.15 shows temperatures recorded for inner and outer TSCs under four different wind speeds with a 4 g initial deposited mass. All lines in Figures 4.15, 4.16 and 4.17 represent average temperatures of three to ten tests. At some wind speeds the inner sensors clearly reach a higher temperature than outer TSCs. Temperatures shown, about 400C, however, are much lower than what would be expected for a smoldering reaction under wind. In this configuration it does not appear the TSCs provide an accurate representation of temperature on the surface of the firebrands, however the sparse nature of the pile may be responsible for poor contact and coverage between the sensors and firebrands. Higher wind speeds to show a slightly higher temperature, owing to higher rates of oxidation at the surface overcoming convective

cooling.

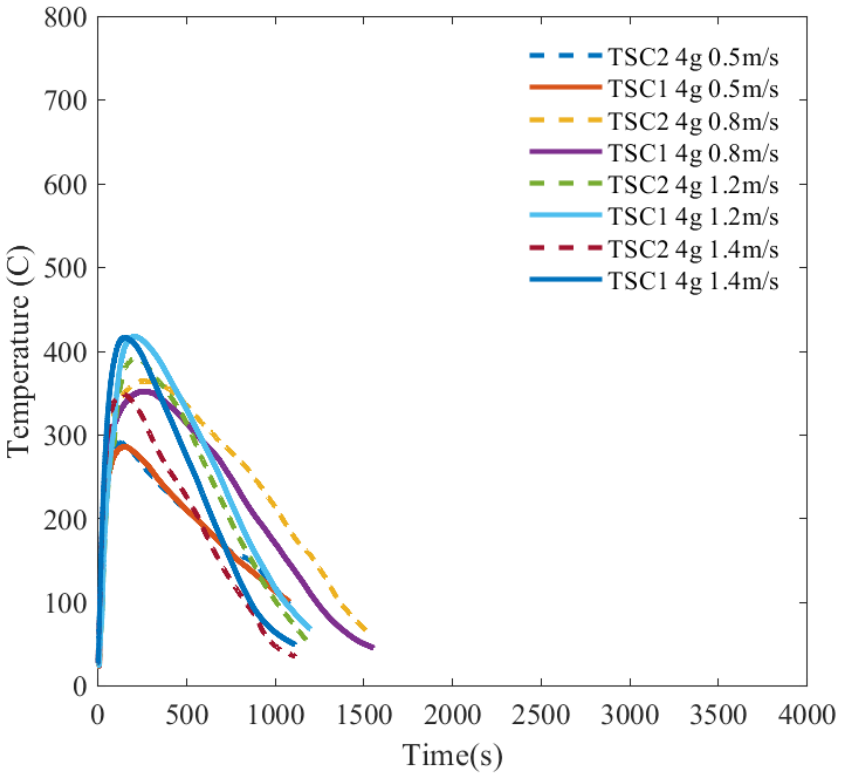

Figure 4.15: Temperatures recorded from TSC sensors in both inner (TSC1) and outer (TSC2) locations below a pile of 4 g of firebrands under different wind speeds.

As shown in Figures 4.15, 4.16 and 4.17, temperatures increase as the deposited mass is increased. The wind speed also appears to have a somewhat stronger effect. When larger piles of firebrands are used sensors remain more completely surrounded, receive re-radiation between the pile, and are also somewhat insulated from convective cooling effects from the surrounding wind. As expected, the heating duration also increases as the deposited mass increases, while the duration of heating slightly

decreases with higher wind speeds owing to faster oxidation rates. .

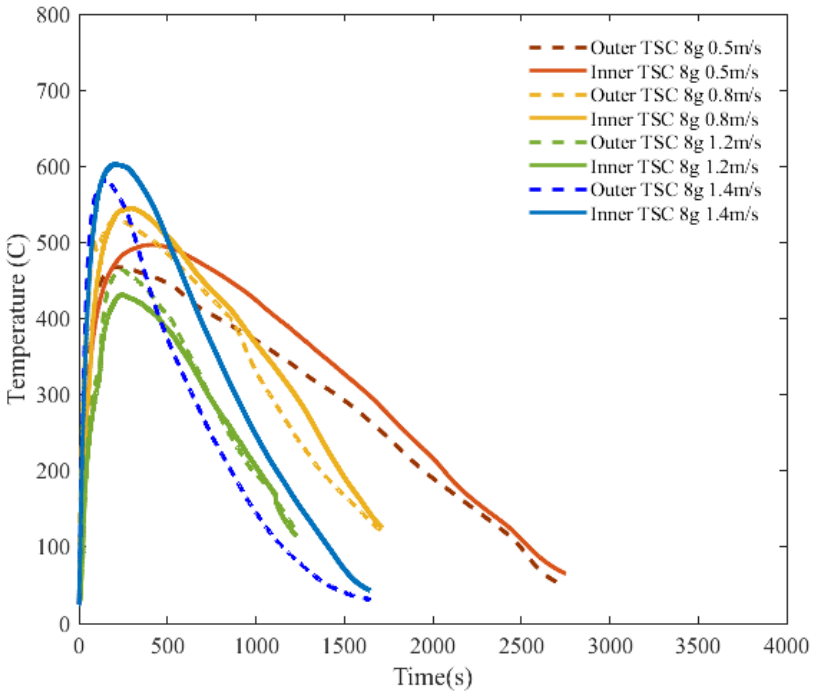

Figure 4.16: Temperatures recorded from TSC sensors in both inner (TSC1) and outer (TSC2) locations below a pile of 8 g of firebrands under different wind speeds.

The difference between inner and outer TSCs is more extreme for larger piles, with the greatest difference about 200°C for the 16 g pile at 1.2 m/s shown in Figure 4.17. While averaged temperatures here reach about 700°C, raw temperatures reach well over 900°C instantaneously at higher wind speeds. These temperatures correspond well with previously measured temperatures by Urban et al. using color pyrometry [45].

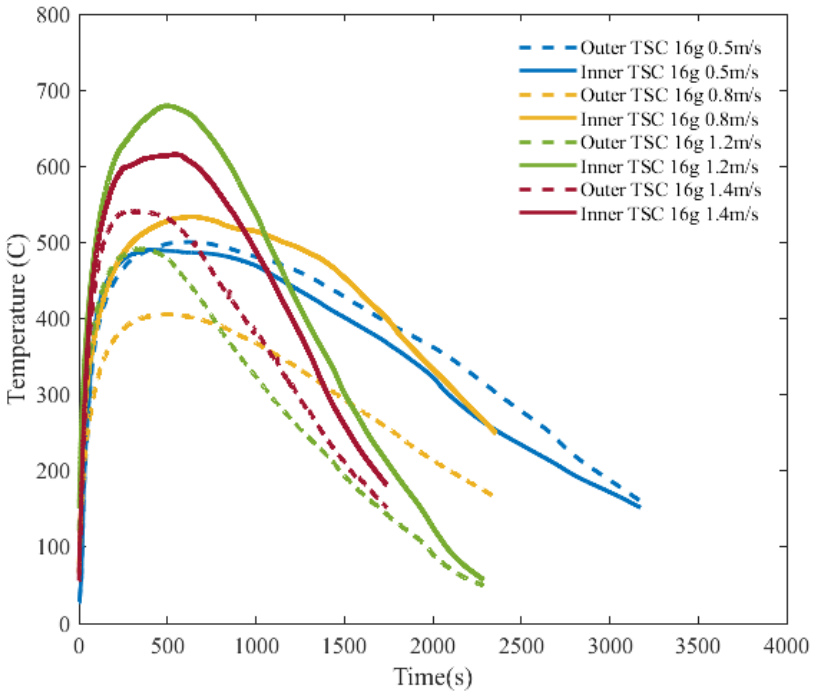

Figure 4.17: Temperatures recorded from TSC sensors in both inner (TSC1) and outer (TSC2) locations below a pile of 16 g of firebrands under different wind speeds.

The significantly higher temperatures with larger piles also suggests that re-radiation may also be important, as larger piles experienced significant glowing that resulted in higher temperatures and heat fluxes beyond what might be expected only by diminishing some convective cooling.

Peak temperatures are shown in Figure 4.18 from the peak of average temperature curves from Figures 4.15, 4.16 and 4.17. As expected, it is seen the peak temperature is related to both the deposited mass and wind speed. Also, the peak temperatures

measured by the inner set of TSCs is higher than those at the outer extend of the pile.

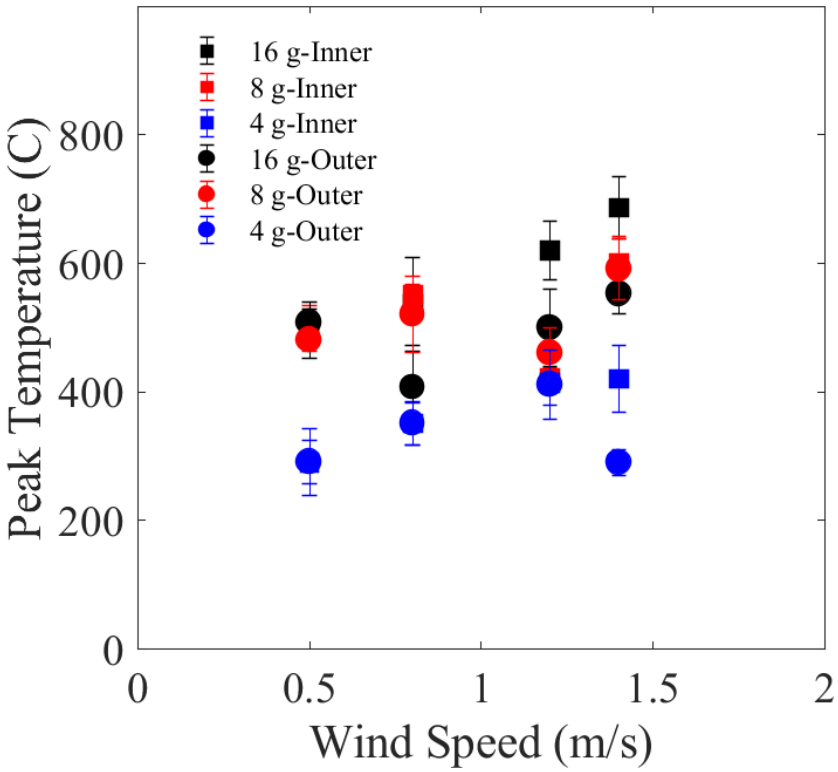

Figure 4.18: Peak Inner and Outer TSC temperatures when 16, 8 and 4 g firebrand deposited for different tests with birch (vendor 1). The peaks were collected from figures 4.15, 4.16 and 4.17. These values are presented on separate graphs for each deposited mass in the appendix

Temperatures are also presented as a spatial map in order to understand how heating changes over the sample surface during experiments with different pile sizes and wind speeds. These heating maps can provide valuable information such as an approximate heating area and a spatial distribution of temperature in a pile

of firebrands. They also confirm the fact that the center of a pile has a higher temperature, and probably heat flux, due to interactions between firebrands. Figures 4.19 to 4.21 show a spatial heating map from for 16 g of deposited mass. The heating maps are shown at $t = 200$ s, a time where most TSC measurements show peak temperatures. In other word, the average value of all 16 thinskins are calculated for each condition at $t = 200$ s and plotted as a heating map in this section.

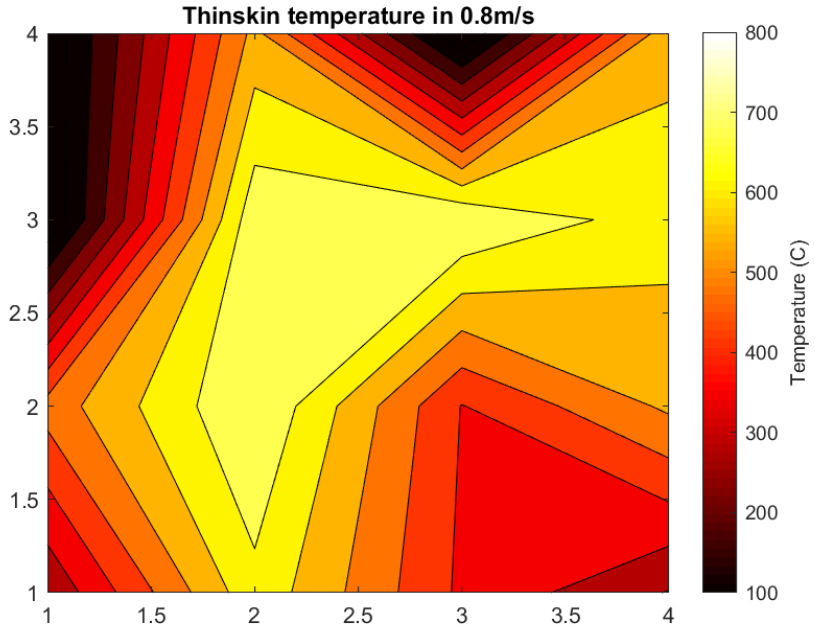

Figure 4.19: Temperatures measured from an array of TSCs presented at $t = 200$ s for 16 g of initial deposited firebrand mass under a wind speed of 0.8 m/s.

As shown in the heating maps, firebrands at the center of a pile have higher temperatures, similar to what was presented in Figures 4.15, 4.16 and 4.17. A full

spatial map, however, reveals been more complex behavior. Either due to the way the pile lands, changes in material properties, or other effects that change over time, heating is in no way uniform and some regions remain considerably hotter or colder than others. When these are played as a function of time these regions move around the pile, indicating that there is a complex, time-dependent aspect to the smoldering process not captured in average measurements.

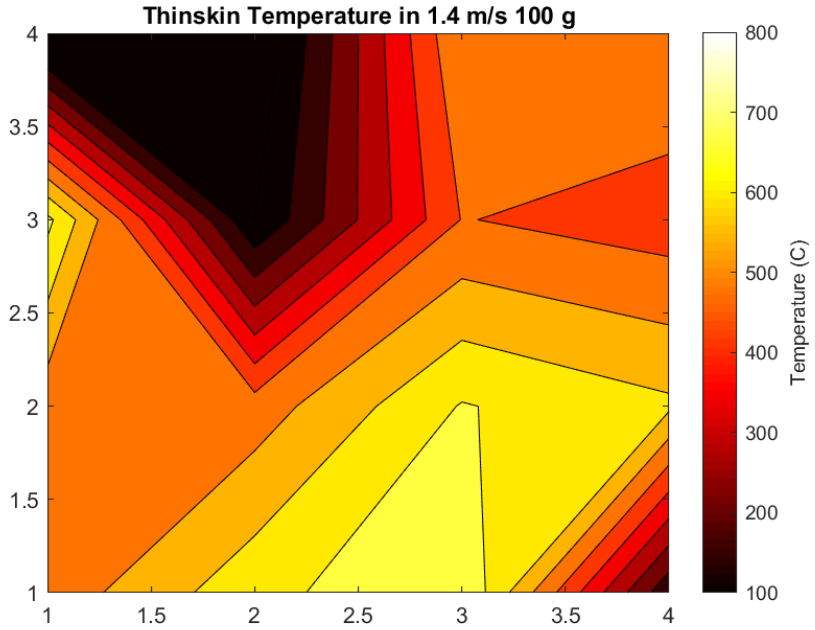

Figure 4.20: Temperatures measured from an array of TSCs presented at $t = 200$ s for 16 g of initial deposited firebrand mass under a wind speed of 1.4 m/s.

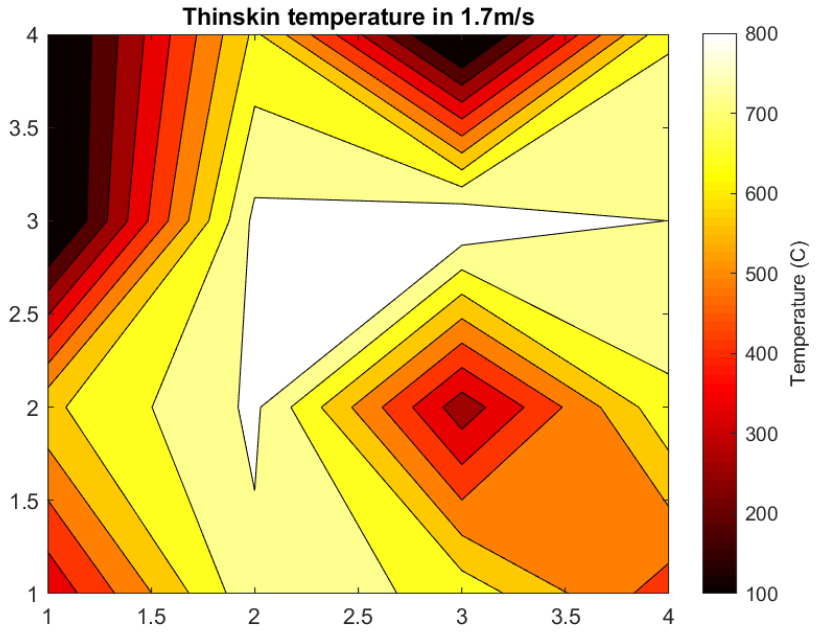

Figure 4.21: Temperatures measured from an array of TSCs presented at $t = 200$ s for 16 g of initial deposited firebrand mass under a wind speed of 1.4 m/s

4.5. Ignition Results

In this section, results from tests over fuel beds with a range of initial densities are presented. Under each wind speed, at least 5 tests were repeated. Ignition occurred in a smoldering condition for almost all cases at a very early stage and propagated into the depth of the fuel. In some cases, especially those with high wind speeds and low recipient fuel density, transition to flaming occurred and flames appeared on the surface of the fuel, observed using videos of recorded experiments. The time to flaming and a representative time to smoldering was determined in each case and used to quantifying ignition conditions for different materials, later to be compared to heat fluxes from inert measurements. As mentioned earlier, the time to smoldering was estimated here as the time when a thermocouple pinned 0.5 cm beneath the top surface of a fuel sample reached 200°C. All samples experienced smoldering on the surface, therefore this definition helped to define a point where smoldering would proceed throughout the sample and not just be maintained by the firebrand pile. The time to flaming was defined as the time at which the flame appeared on the top of the fuel bed. The density of the fuel bed was ultimately found to be a critical parameter related to propensity of ignition.

The density of fuels were determined in a fully dried condition using five samples of each type. Dimensions of each sample were measured by calipers and the mass of

each sample was measured using a load cell with an accuracy of 0.1 grams. Density was calculated with knowledge of mass and volume for each sample. Average value from five samples of each material was used in all calculations and graphs, and are also shown in table 4.

Table 4: Fuel Measured Densities $[kg/m^3]$

Sample	MGP	OSB	Cedar
1	571	680	310
2	572	645	312
3	548	660	304
4	554	665	299
5	582	663	301
average	565.4±12.51	662.6±11.18	305.2±5.03

4.5.1. Time to Smoldering

The time to smoldering was calculated from thermocouple (TC) data and is the time when the TC temperature reached 200°C. This limit was chosen by comparing plots from ignition tests with samples after ignition tests presented in Chapter 3. The reason the estimated smoldering temperature is much less than real smoldering temperatures is that, although thermocouples were in touch with wood samples at

the beginning of each test, when ignition reached near thermocouples, they were detached from wood upon ignition of the wood. A smoldering propagation rate could be calculated knowing the vertical depth of the thermocouple from the fuel surface and the time the TC reached an estimated smoldering temperature, shown in Figure 4.22. These are later converted into a time by removing the depth of the thermocouple for later comparisons with flaming ignition.

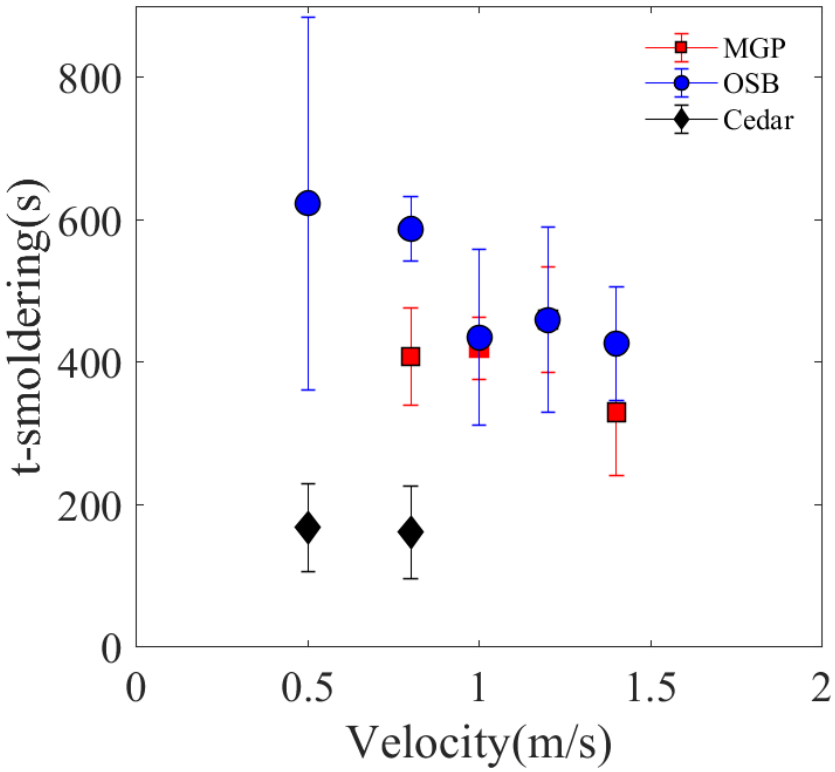

Figure 4.22: Time to smoldering calculated using an in depth thermocouple for three fuel samples, marine grade plywood (MGP), oriented strand board (OSB) and cedar wood.

It was found that the density of the fuel plays an important role in the smoldering

propagation rate. A higher fuel density resulted in lower smoldering rates. When the wind speed increases, the smoldering rate also increases and becomes more repeatable than somewhat stochastic tests at lower wind speeds, as shown in Figure 4.22. This trend will continue for flaming conditions discussed in the next section.

4.5.2. Critical Heat Flux at Smoldering

The main goal of this study was to determine the heating conditions preceding ignition of different solid fuel beds under both smoldering and flaming conditions. Critical heat fluxes were determined from WC-HFG readings taken in Section 4.2 at the time of ignition. The heat flux was extracted, however at time when thinskin temperatures reached the ignition temperature of wood, as matching ignition times directly did not produce clear results. Knowing the fact that temperature of thinskins are not equal to temperature of fuel, heat flux at time when TSC temperature reached ignition temperature of fuel is used to determine critical heat flux value. This method is not suitable to determine the exact value of heat flux. However, these values of heat flux can represent a comparison for critical heat fluxes in different fuels. Babrauskas [46] presented ignition temperatures of 300-310°C for hardwoods. Also Yudong [47] measured ignition temperatures of wood samples with different densities and presented the ignition temperature of wood varies between 311-354°C when the density of wood is 0.33-0.64 g/cm^3. In this research, an ignition temperature of

310-350°C is used for different fuels, depending on their densities.

Heat fluxes from WC-HFG data was extracted at the moment when TSC data reached those temperatures. It is presented in Figure 4.23 that the critical heat flux at ignition for all three fuels are close since they have a relatively close pyrolysis temperature. Although this method will not provide exact values for critical heat flux, it is still a methodology to compare the critical heat flux for different fuel beds.

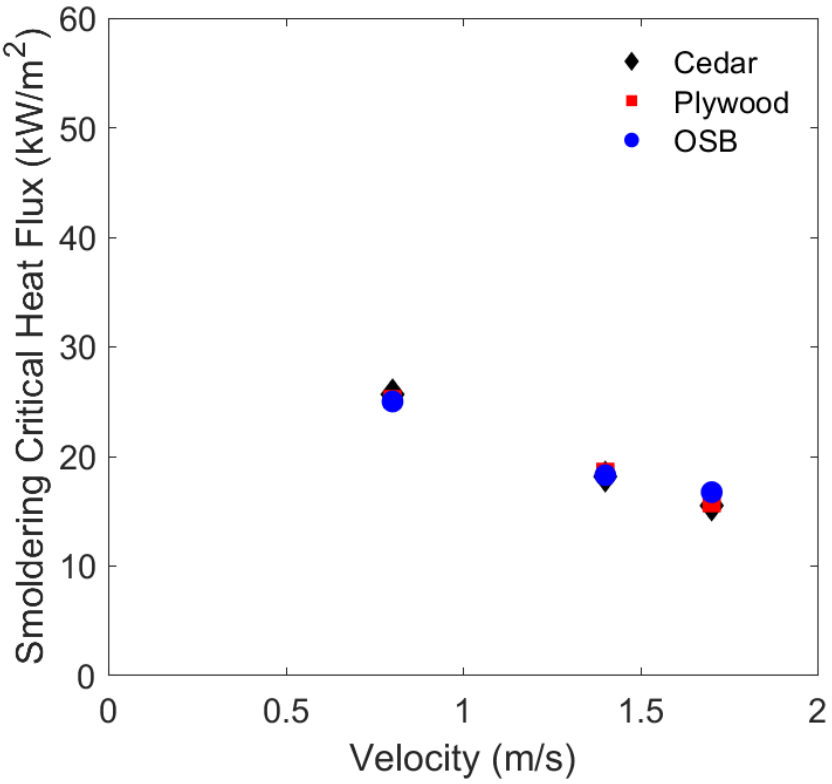

Figure 4.23: Critical heat fluxes estimated at the onset of smoldering.

4.5.3. Time to Flaming

The time to flaming was also determined. Many factors affect ignition conditions, such as wind speed, firebrand deposited mass and fuel density, which may lead not only to ignition of the fuel but to later transition to a flaming condition. In order to characterize this phenomena, the time to flaming and flaming propensity are defined and presented in Figure 4.24 for different fuel beds and wind speeds. Under a certain wind speed and firebrand loading condition not all tests may transition to flaming, therefore the flaming propensity is introduced in Figure 4.24 as a ratio of the number of tests which transitioned to flaming versus the number which did not. This is shown as different colored shadings, with darker colors indicating more likelihood of transition. Ultimately, higher wind speeds were more likely to transition to flaming, as expected. Lower wind speeds also experienced more variability for fuels that sometimes only smoldered and sometimes transitioned to flaming.

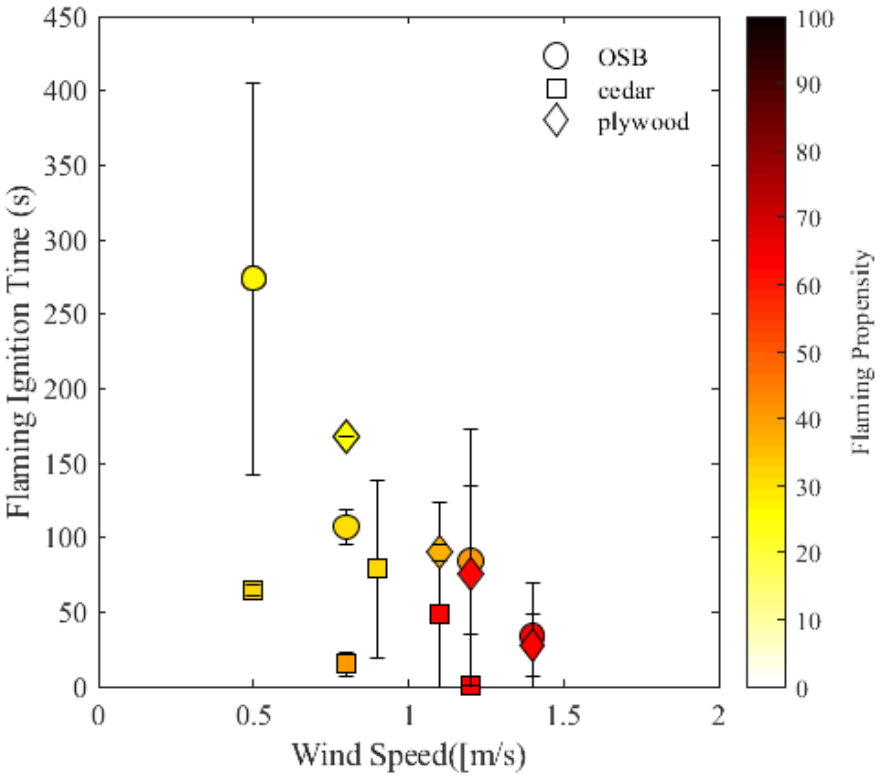

Figure 4.24: Time to flame observed from videos. Each average is taken from at least 5 repeated tests. The color-shaded propensity shows the percentage that flaming occurred. In all tests, 16 grams of firebrands were deposited.

The time to flaming was measured from the beginning of each experiment to the moment when the flame appeared on the fuel surface. Under low wind speeds, the probability of flaming on the fuel surface is low, especially when fuel density is high.

Figure 4.25: Transition from smoldering to flaming of the fuel bed.

It is important to distinguish the initiation of flaming over the pile of firebrands versus over the fuel surface. Flames were observed in both scenarios, over the firebrand pile and forming directly adjacent to fuels. It was found that flames over firebrand piles usually started at the top of the pile and moved to the left of pile (downwind). However, flames starting over the surface fuel typically started at the boundary of the fuel and pile of firebrands, at the right side of the pile (upwind). Figure 4.26 shows flames observed over firebrands and the fuel surface.

Figure 4.26: Photograph showing flames present both over the pile of firebrands and over the fuel surface.

4.5.4. Critical Heat Flux at Flaming

The critical heat flux for flaming ignition was determined by matching the time to flaming from Figure 4.24 and the heat flux from WC-HFG data. This critical heat flux depends on fuel bed density and wind speed when a single firebrand loading condition, i.e deposited mass, firebrand type and contact area, was used and repeated for different fuel types.

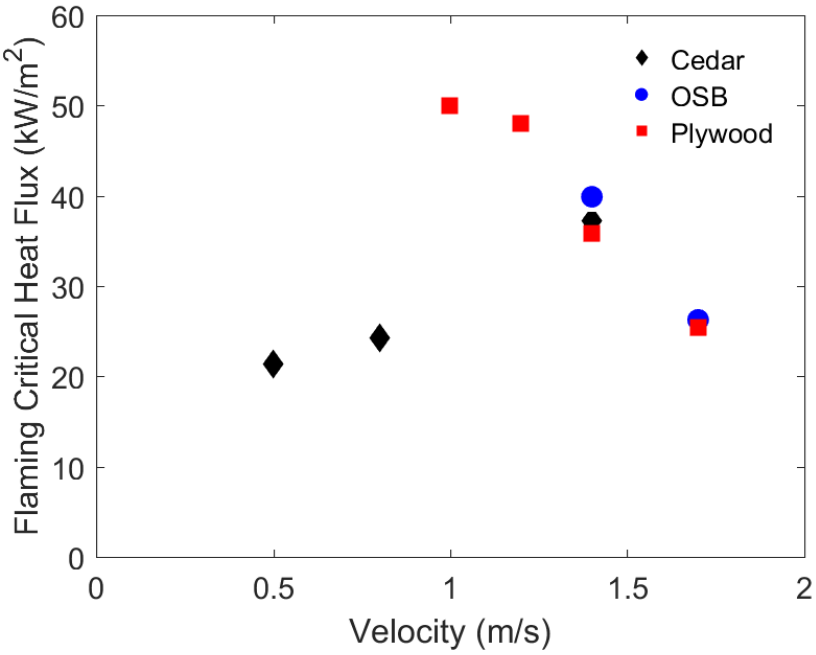

Figure 4.27: Critical heat flux determined at the time to flaming.

The critical heat flux determined from heat flux data presented in Section 4.2 at the time to flaming is presented in Figure 4.27. It is clear that flaming critical heat fluxes are larger than smoldering critical heat fluxes in most cases since more thermal energy is needed to establish flaming in the combustion reaction. Different trends are also revealed between different fuels. Cedar, for instance, requires higher critical heat fluxes at higher wind speeds to transition to flaming, however the trend is the opposite for plywood. Many questions remain to be answered, most likely necessitating a better understanding of the interaction of different components of heat transfer and the makeup of different fuels.

Chapter 5: Discussion

5.1. Wind Effects

Wind was found to be one of the most important factors affecting ignition of fuel beds when firebrands are deposited over them. Flaming may not occur on many dense fuel beds when there is no wind (even in large piles). Higher winds affect fuels by increasing rates of oxidation, allowing for more oxygen availability during the progression of these solid phase reactions. This is seen in resulting heat flux and temperature measurements at higher wind speeds. Changes with pile sizes also are interesting, suggesting there may be significant re-radiation effects which need to be investigated further.

The higher heat fluxes and temperatures don't present the whole story, however. With faster rates of reaction burnout also occurs faster, resulting in shorter heating duration. To achieve ignition, the right combination of high heat flux with enough time to impart that heat flux must be achieved. It is a challenge to condense this heavily time-dependent data, but some first steps were approached here.

In this research, wind speeds varied from 0.5 m/s to 2 m/s during the experiments. Since the wind tunnel used in experiments were not be able to produce wind speed condition lower than 0.5 m/s and also the effect of wind speed lower than 0.5 m/s

is found similar to no wind condition. Also when the wind speed is higher than 2 m/s, the firebrands are likely to travel by wind which is not the case study in this research since this work is focused on landed firebrands and not traveling embers.

5.2. Scaling Analysis

5.2.1. Smoldering Condition

Smoldering ignition times were determined, as described in Chapter 3, using embedded thermocouples. To couple these results into a use able form, the dominant parameters are first delineated. Based on these results it is seen that ignition is a function of the firebrand deposited mass, wind speed, and density of fuel. It is also thought that the contact area and thickness of fuel could also play a role. The ignition time, t_s, is therefore could be represented as

$$t_s = f(q_p'', m, U_\infty A_c, \alpha, \delta, \rho_f, \rho_F), \tag{3}$$

where q_p'' is the heat flux at the pyrolysis ignition condition, m is the firebrand deposited mass, U_∞ is the wind speed, A_c is the contact area between firebrand and fuel,α is the thermal difussivity of fuel,δ is the thickness of fuel,ρ_f is the density of firebrand and ρ_F is the density of fuel.

It is desired to express these parameters in a non-dimensional form. Several

existing non-dimensional variables are approached, first the Fourier number,

$$Fo = \alpha t_s / \delta^2 \tag{4}$$

where t_s is time to smoldering, α is the thermal difussivity of fuel and δ is the thickness of fuel. This converts a characteristic time as a function of the conduction heat transfer into the fuel to be ignited. Heat flux is also important and is non-dimensionalized.

$$q^* = mU_\infty^3 / CA_c^{1.5} \tag{5}$$

where $q^{*\prime\prime}$ is the non dimensional heat flux, m is the firebrand deposited mass, U_∞ is the wind speed, A_c is the contact area between firebrand and C is the correlation between peak heat flux and wind speed in the units of [W] presented in figure 4.6.

Finally, the density of the fuel to the firebrands is normalized,

$$\rho^* = \rho_F / \rho_f \tag{6}$$

To find a correlation between these parameters, their values were calculated for each ignition experiment and shown in Figure 5.1. Different fuel types are indicated and a linear fit is shown between the data. Since an average smoldering time was used for each test condition, error bars are presented for each condition which represent

the standard deviation in Fo, due to variation in the ignition time.

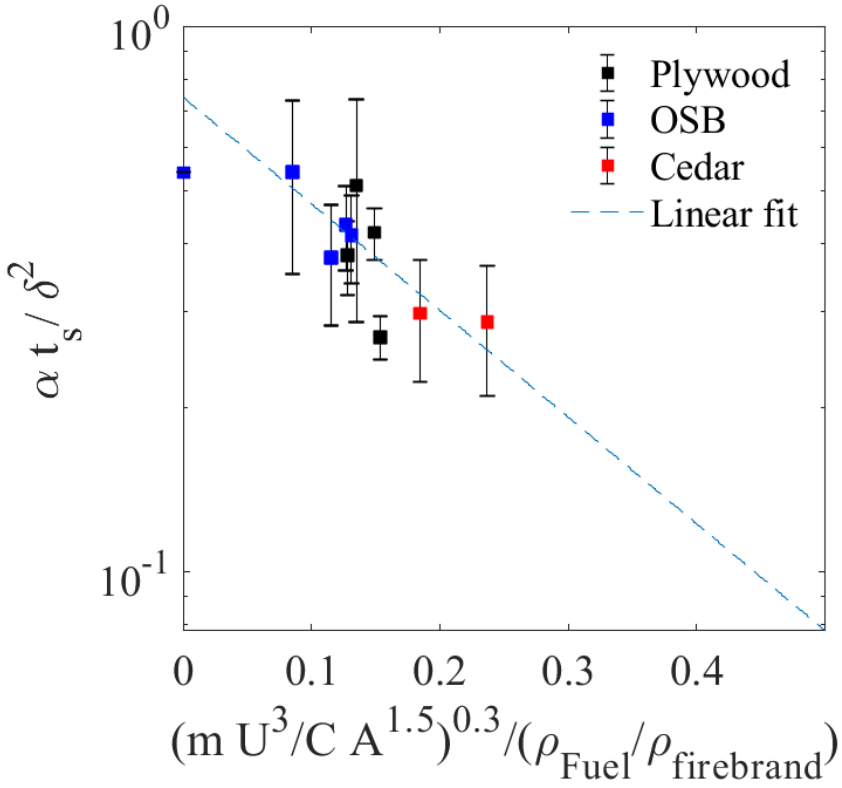

Figure 5.1: Experimental data fitted on scaling analysis

Using a linear fit between the data in Figure 5.1, a correlation between these parameters is shown as follows,

$$Fo = 0.74exp(-4.5q^{*0.3}/\rho^*) \qquad R^2 = 0.5086 \quad (7)$$

The R^2 value is relatively low, indicating a poor degree of fit, however there is a somewhat consistent trend of decreasing ignition time with the fuel ignition parameter, notably density.

5.2.2. Flaming Condition

The time to flaming ignition (t_f), which represents the time it takes from the moment of depositing firebrands over a fuel bed to the moment that flames appear on the surface of the fuel was determined as a function of the same parameters as smoldering, but replacing smoldering values with those from flaming ignition.

Experimental data was plotted on semi logarithmic graph where Fo calculated from experiments with different conditions is plotted against $q^{*0.3}/\rho^*$. A linear trend is shown between Fo and $q^{*0.3}/\rho^*$ when they are plotted on semi logarithmic graph,

$$Fo = 1.4716exp(-19.16q^{*0.3}/\rho^*) \qquad R^2 = 0.8614(8)$$

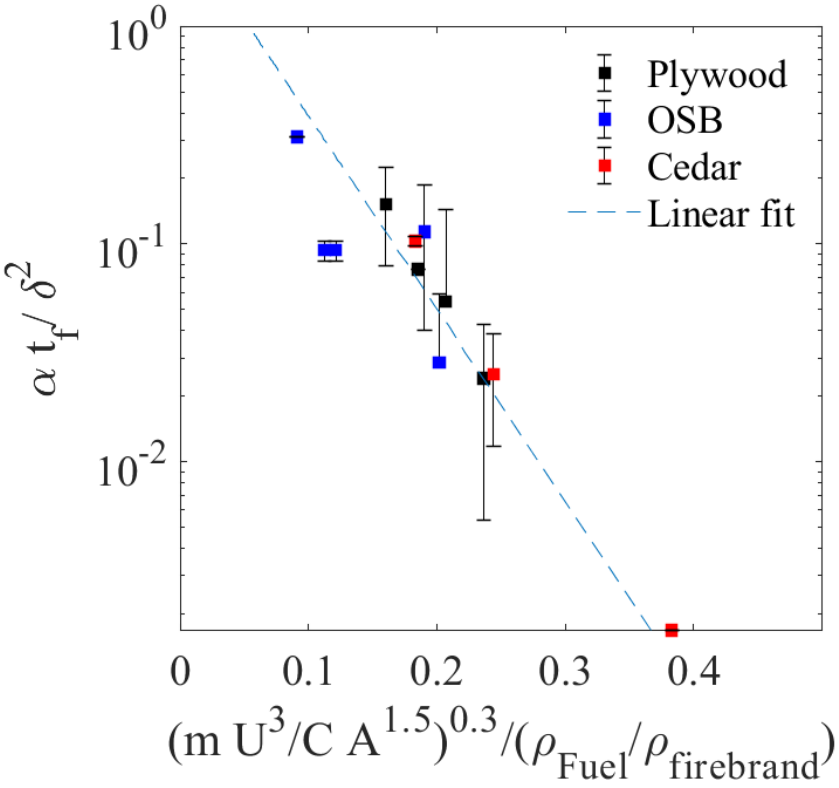

Figure 5.2: Experimental data fitted on scaling analysis

This correlation follows a much higher degree of fit, perhaps because the time to flaming is much easier to define and capture. It can be concluded from this simple analysis that the time to flaming increases with higher fuel density, lower firebrand density, lower firebrand deposited mass, lower wind speed, lower peak heat flux and lower thermal diffusivity of fuel and since thermal diffusivity of fuel depends on density of fuel (higher the later lower the former). Density was found to be the most important parameter of the fuel to define time to flaming.

Both smoldering and flaming conditions are plotted together in Figure 5.3, with a non-dimensional parameter of heating on the x-axis starting from 0 first with a smoldering condition. When it reaches about 0.1, transition from smoldering to flaming started with a low flaming probability. As it gets larger, transition to flaming always occurs and Fo starts to decrease logarithmically.

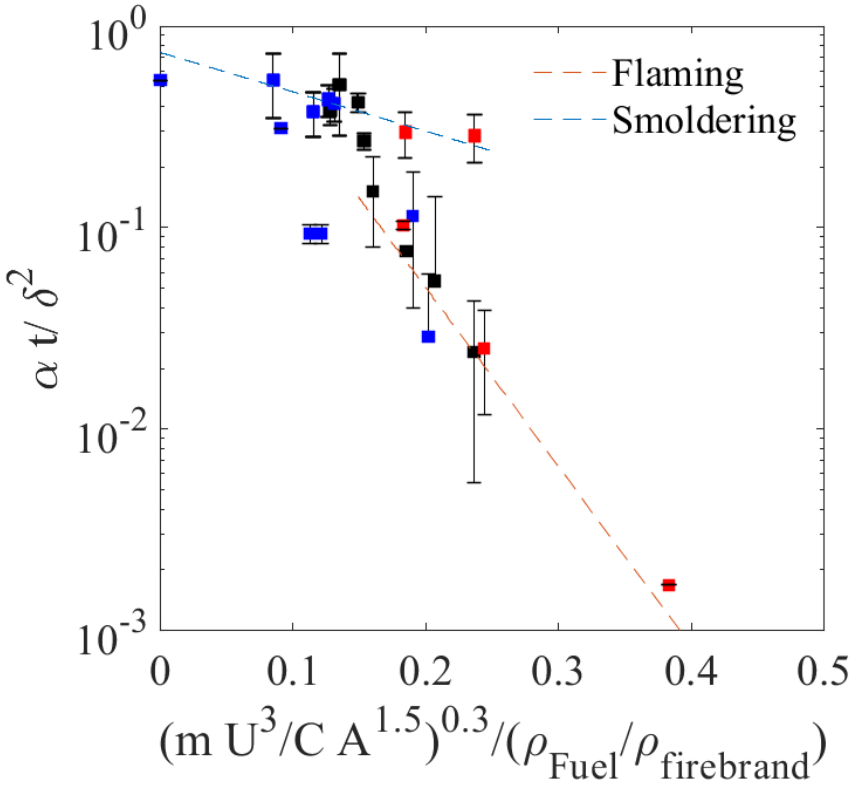

Figure 5.3: Experimental data fitted on scaling analysis

Chapter 6: Conclusion

6.1. Summary

A methodology was developed to examine the influence of piles of smoldering firebrands on ignition of dense fuel beds under wind speeds from 0.5 to 2 m/s. Two series of parallel tests were conducted over a sensor array and three different solid fuel beds. A methodology was used to determine the heat flux and temperature of a pile of firebrands in smoldering conditions and quantify ignition condition of the fuel beds.

6.2. Conclusion

Several factors were found to be critically important to the ignition of fuel beds, namely the ambient wind speed, pile mass, and density of both initial firebrands and fuel beds. While this study takes an enormous number of experiments and repetitions due to the stochastic nature of transition to flaming and variability in wood samples, some trends were still extracted from these experiments. Temperatures and heat fluxes rise under increased wind speeds, which is critically important, and similar effects are seen on ignition conditions. Increasing wind speeds result in more rapid oxidation in firebrands and ignited fuel beds and increases temperatures, starting

the transition to flaming in both fuel beds and firebrands when this occurs. In terms of ignition, the density of the fuel bed was found to be most important.

Numerous factors were not considered in this study. For one, a flat surface is the simplest geometry possible and not representative of the real world. It still presents a perfect configuration for fundamental study, but future work will have to address more complex geometries. The moisture content of the fuel was also fixed near 0, which is a worst-case scenario but somewhat unrealistic.

Results point to interesting interactions between firebrands once they are deposited in bulk over a surface. In this situation, firebrands at the center of a pile have higher temperatures than surrounding firebrands, which are losing heat to the surrounding environment. This overcomes some cooling effects but still causes increased temperatures and heat fluxes with higher wind speeds. The role of re-radiaiton within the pile was not explored, but may be important here.

6.3. Future Work

Many factors play an important role on the ignition of fuel beds. While the effects of some factors have been illustrated in this research, there are other factors that should be studied in future works. Firebrand shape is one important factor that has not been studied in this research. Cylindrical firebrands were the only firebrand shape that has been studied and other shapes such as disks should be

tested to determine the effect of firebrand shape. Also, the moisture content of fuel beds remained zero in all experiments in this research. This change in MC may not have a negligible effect on the ignition of fuel beds and should be studied in future works. Also, the wind speed was varied from 0.5-2 m/s in all experiments and heat flux trends for those wind conditions were illustrated. It is important to consider conducting experiments with higher wind speeds which may have cooling effects on the glowing firebrands.

Finally, as mentioned earlier, other geometries such as crevices, L-shaped walls, and corners are more common accumulation points in real fires than the flat surfaces studied here. Although this study provides fundamental information on ignition, it's important to understand how changes in geometry may result in different effects on ignition.

Chapter 7: Appendix

7.1. Heat flux Results

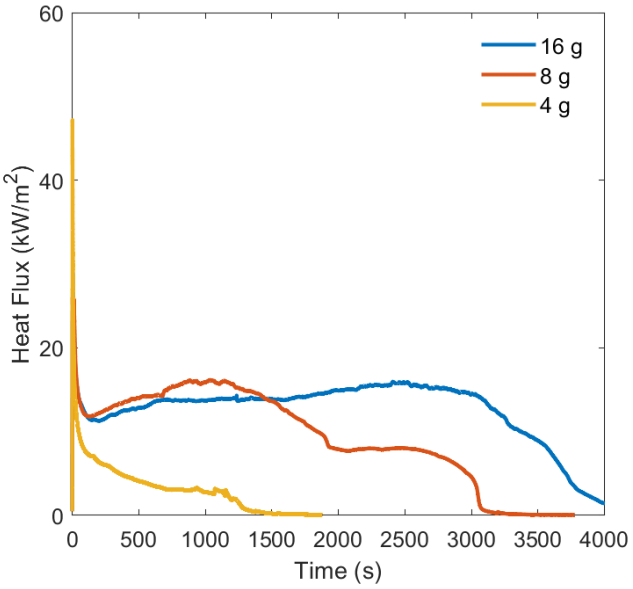

Figure 7.1: Average heat flux for different deposited mass when wind speed is 0.5 m/s

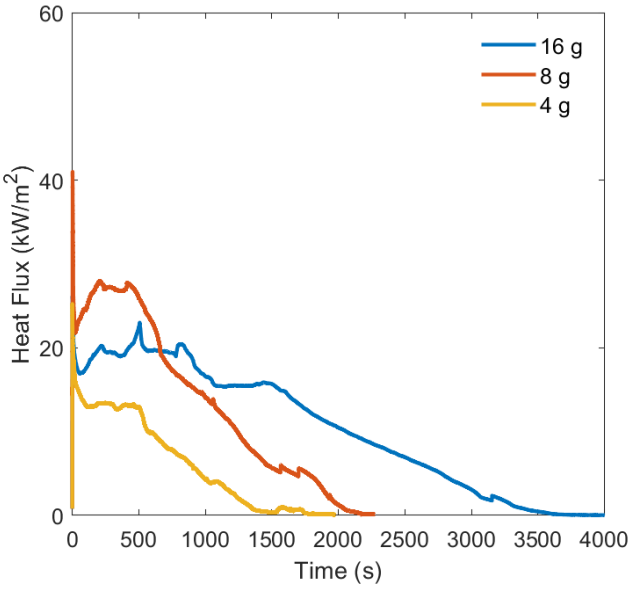

Figure 7.2: Average heat flux for different deposited mass when wind speed is 0.8 m/s

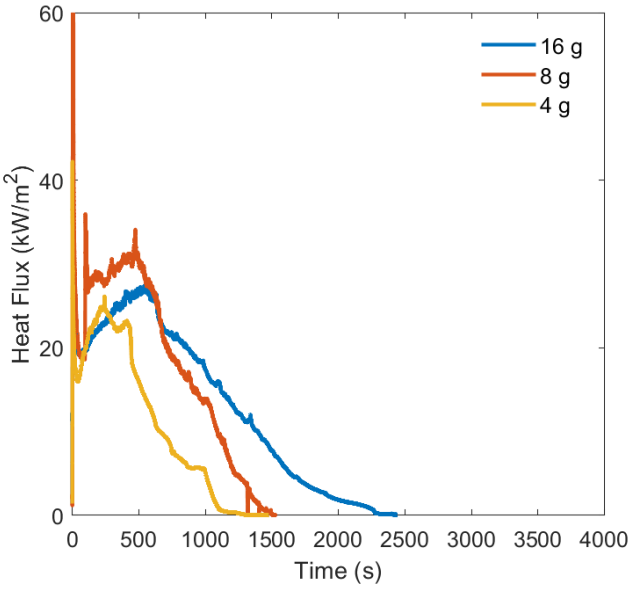

Figure 7.3: Average heat flux for different deposited mass when wind speed is 1.2 m/s

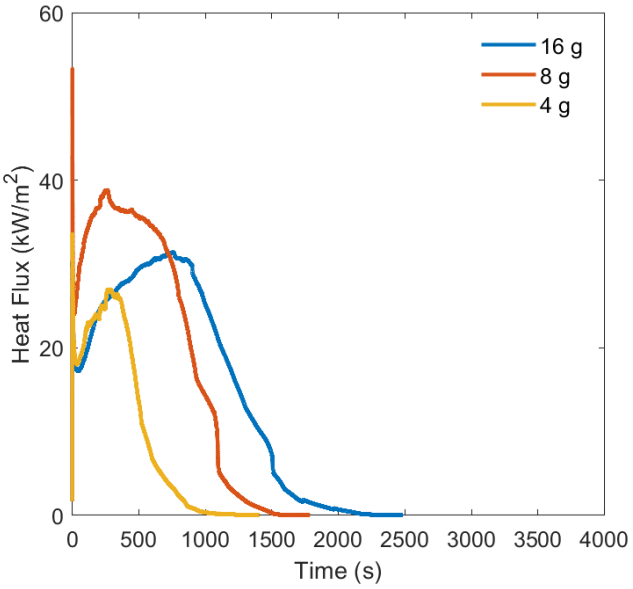

Figure 7.4: Average heat flux for different deposited mass when wind speed is 1.4 m/s

7.2. TSC data

Figure 7.5: TSC data for wind speed of 0.5 m/s when 4 g firebrand were deposited.

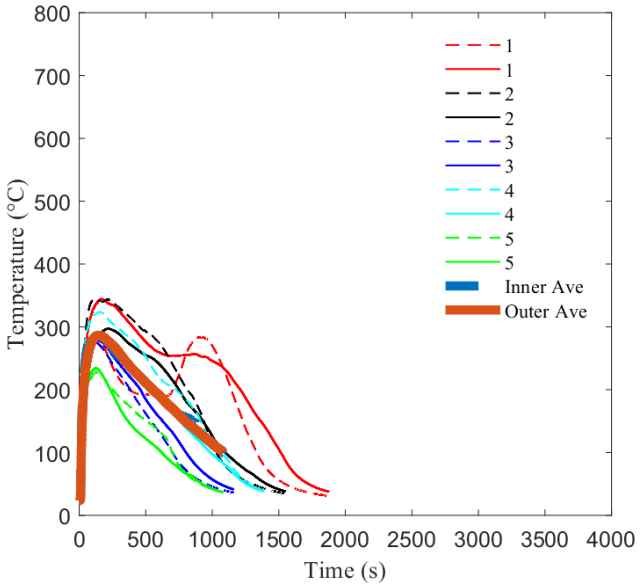

Figure 7.6: TSC data for wind speed of 0.5 m/s when 8 g firebrand were deposited.

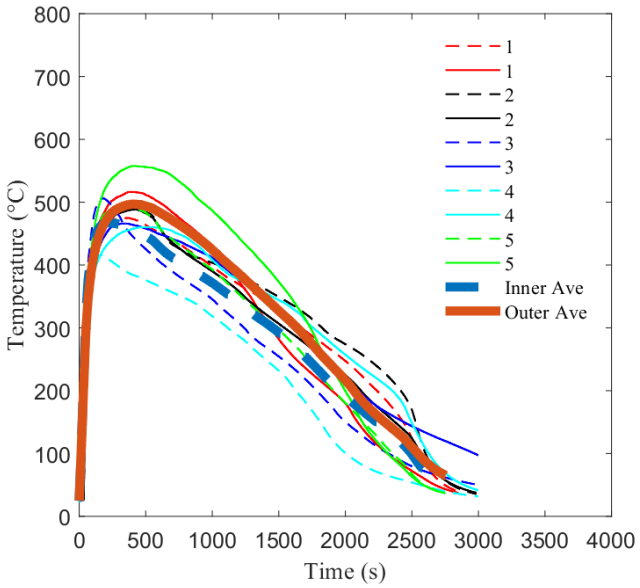

Figure 7.7: TSC data for wind speed of 0.5 m/s when 16 g firebrand were deposited.

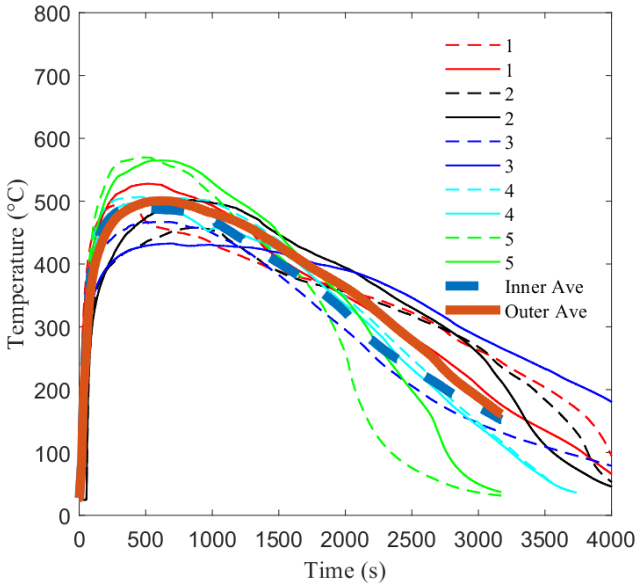

Figure 7.8: TSC data for wind speed of 0.8 m/s when 4 g firebrand were deposited.

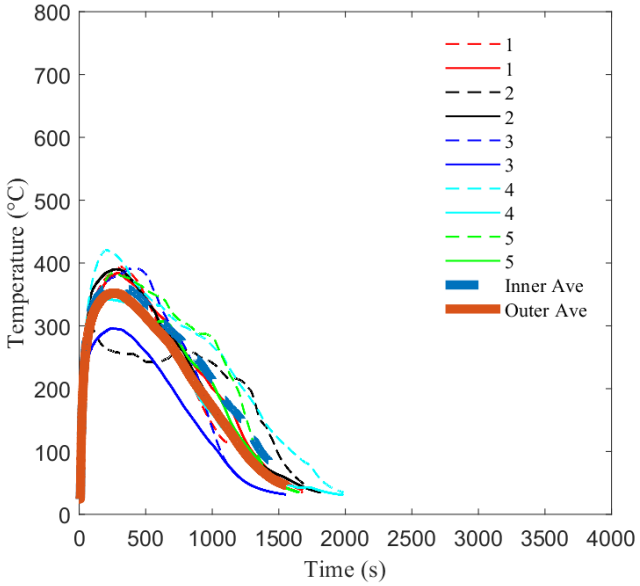

Figure 7.9: TSC data for wind speed of 0.8 m/s when 8 g firebrand were deposited.

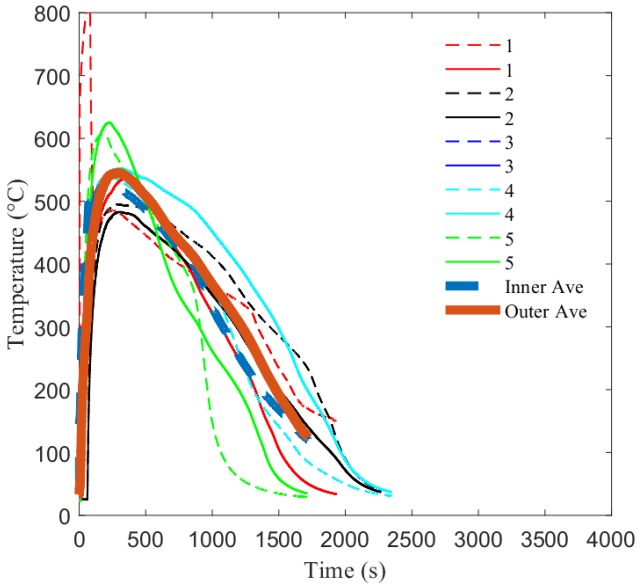

Figure 7.10: TSC data for wind speed of 0.w m/s when 16 g firebrand were deposited.

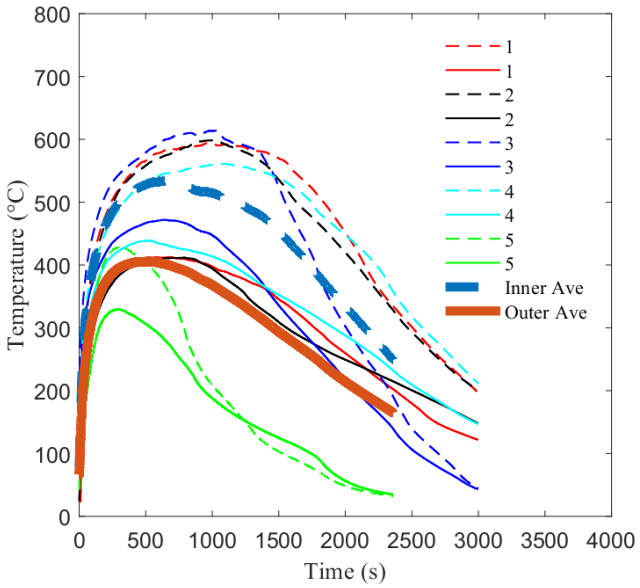

Figure 7.11: TSC data for wind speed of 1.2 m/s when 4 g firebrand were deposited.

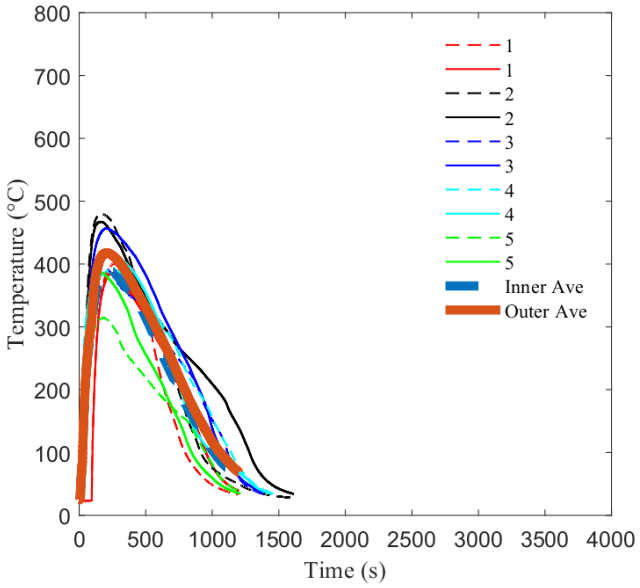

Figure 7.12: TSC data for wind speed of 1.2 m/s when 8 g firebrand were deposited.

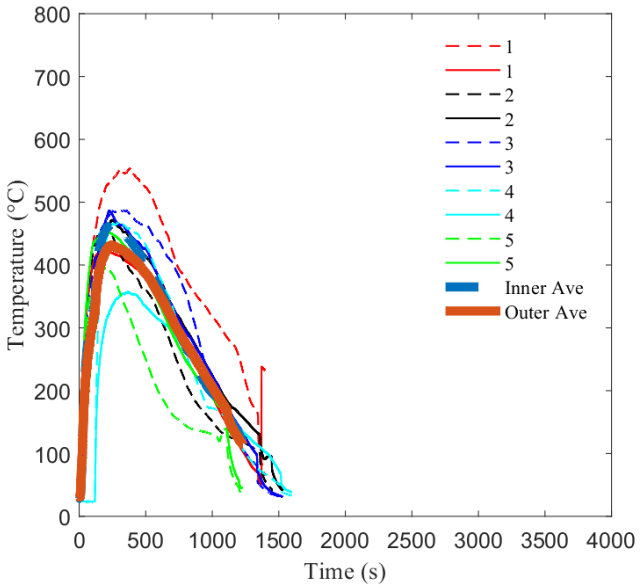

Figure 7.13: TSC data for wind speed of 1.2 m/s when 16 g firebrand were deposited.

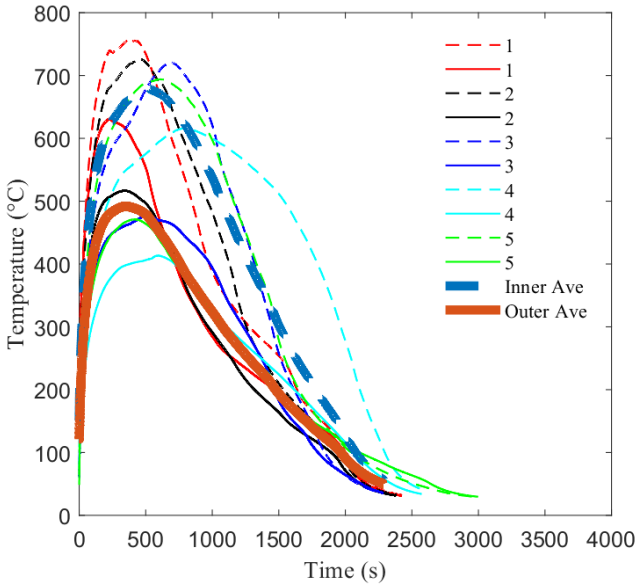

Figure 7.14: TSC data for wind speed of 1.4 m/s when 4 g firebrand were deposited.

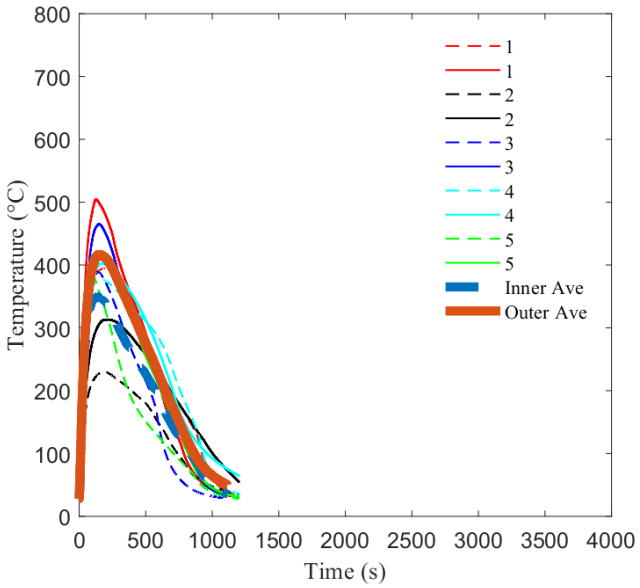

Figure 7.15: TSC data for wind speed of 1.4 m/s when 8 g firebrand were deposited.

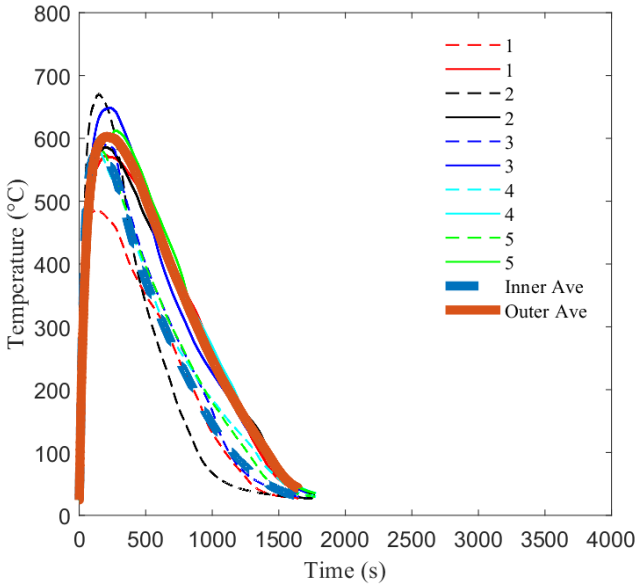

Figure 7.16: TSC data for wind speed of 1.4 m/s when 16 g firebrand were deposited.

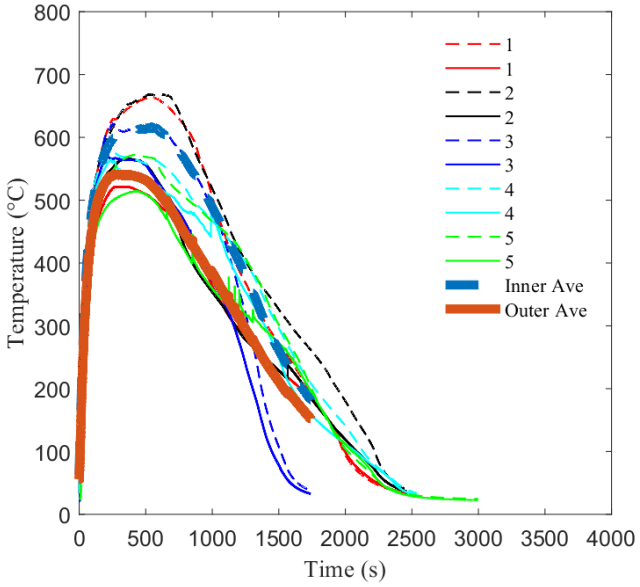

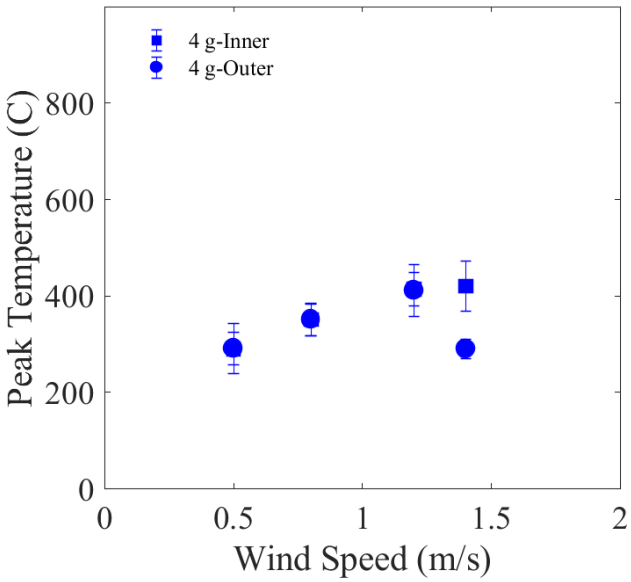

Figure 7.17: Peak inner and outer temperature from average TSC data for each wind speed when 4 g firebrand is deposited over fuel.

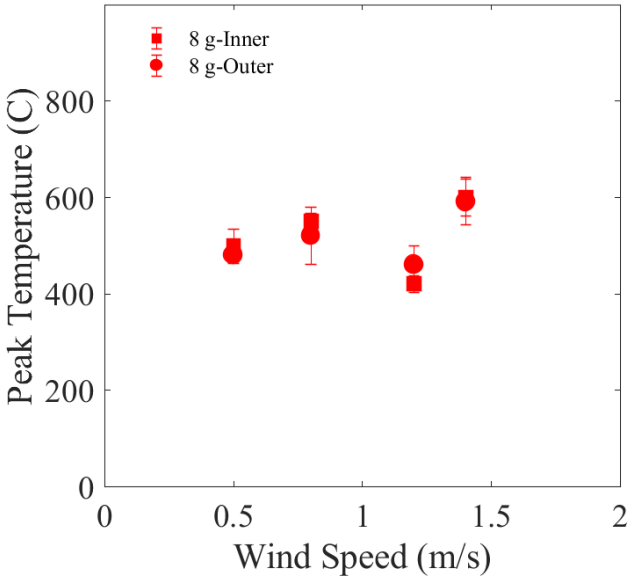

Figure 7.18: Peak inner and outer temperature from average TSC data for each wind speed when 8 g firebrand is deposited over fuel.

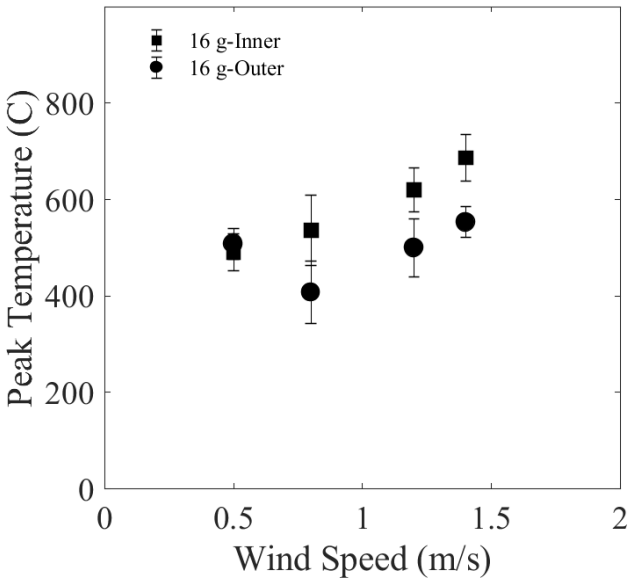

Figure 7.19: Peak inner and outer temperature from average TSC data for each wind speed when 16g firebrand is deposited over fuel.

Figure 7.20: TSC data for wind speed of 0.5 m/s when 4 g firebrand were deposited.

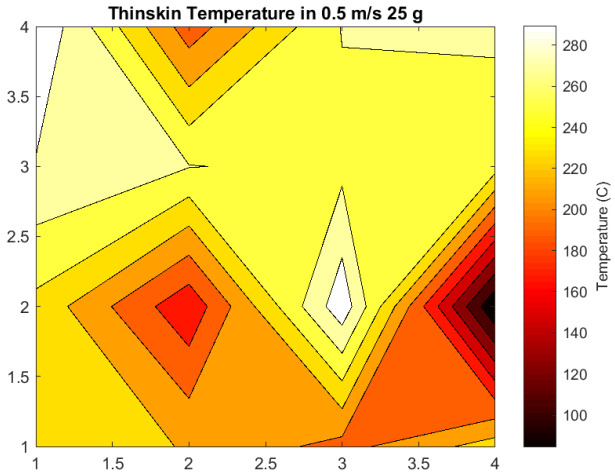

Figure 7.21: TSC data for wind speed of 0.5 m/s when 8 g firebrand were deposited.

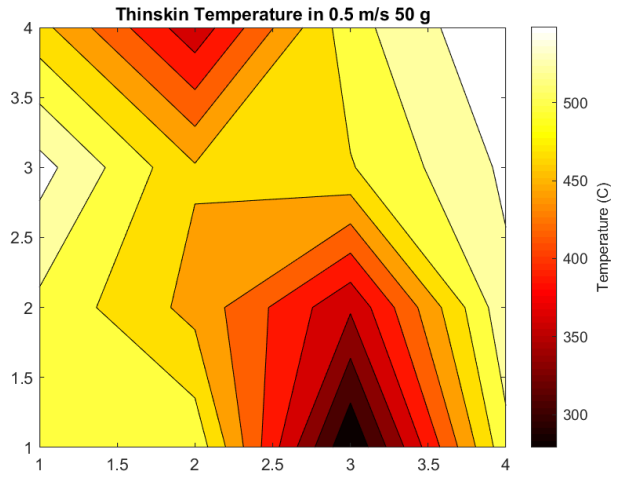

Figure 7.22: TSC data for wind speed of 0.5 m/s when 16 g firebrand were deposited.

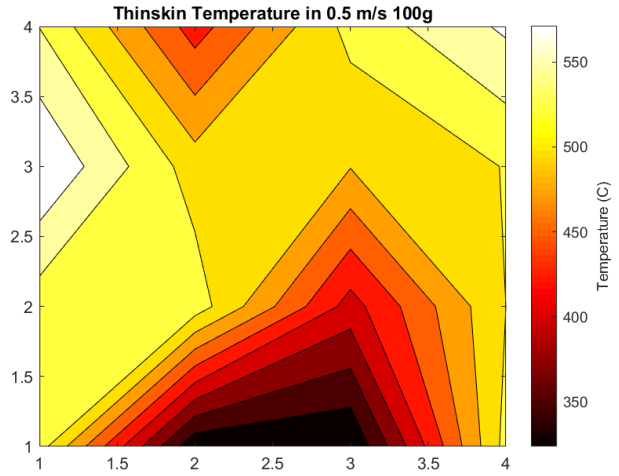

Figure 7.23: TSC data for wind speed of 0.8 m/s when 4 g firebrand were deposited.

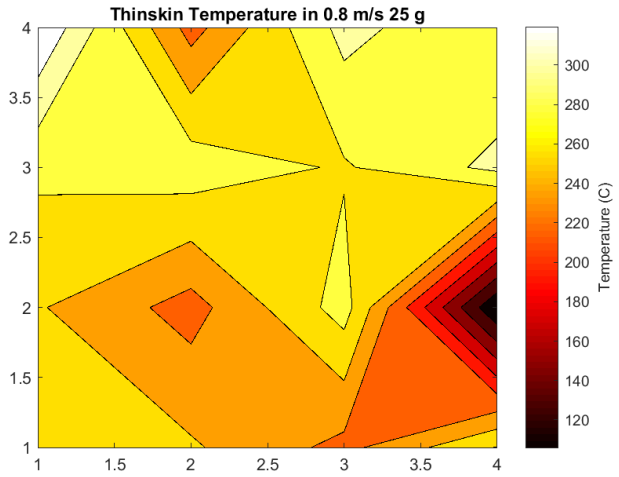

Figure 7.24: TSC data for wind speed of 0.8 m/s when 8 g firebrand were deposited.

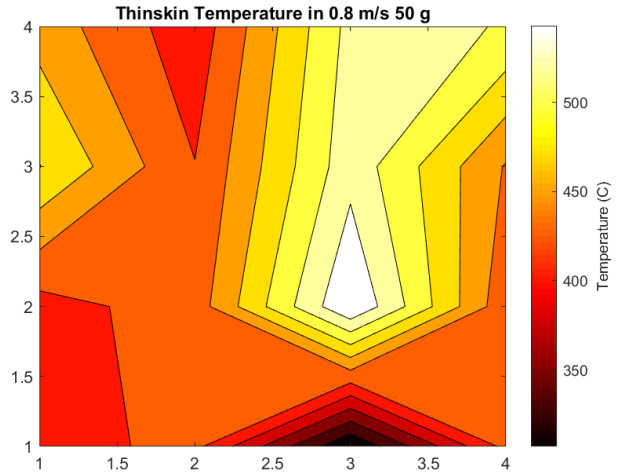

Figure 7.25: TSC data for wind speed of 0.8 m/s when 16 g firebrand were deposited.

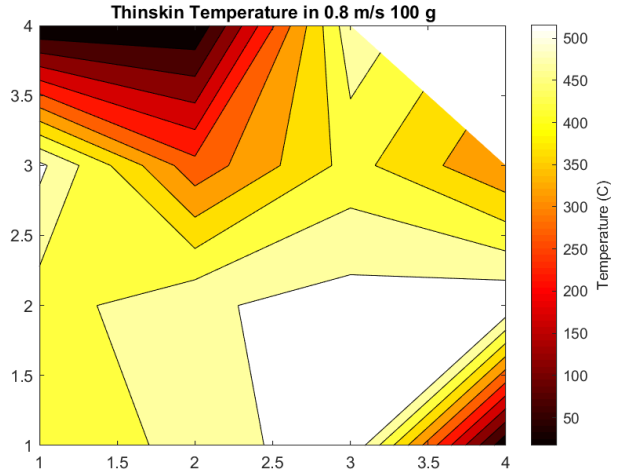

Figure 7.26: TSC data for wind speed of 1.2 m/s when 4 g firebrand were deposited.

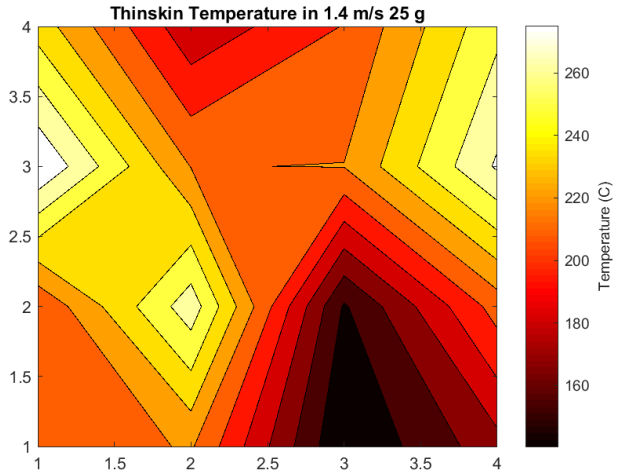

Figure 7.27: TSC data for wind speed of 1.2 m/s when 8 g firebrand were deposited.

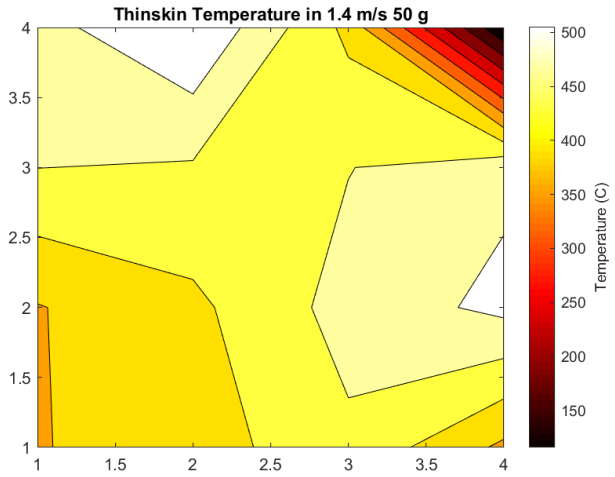

Figure 7.28: TSC data for wind speed of 1.2 m/s when 16 g firebrand were deposited.

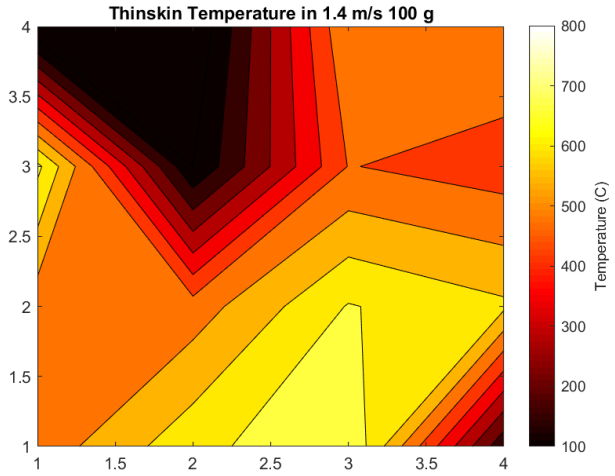

Figure 7.29: TSC data for wind speed of 1.4 m/s when 4 g firebrand were deposited.

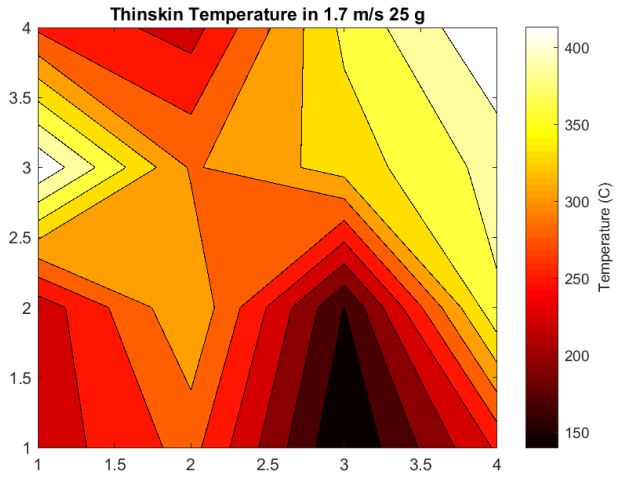

Figure 7.30: TSC data for wind speed of 1.4 m/s when 8 g firebrand were deposited.

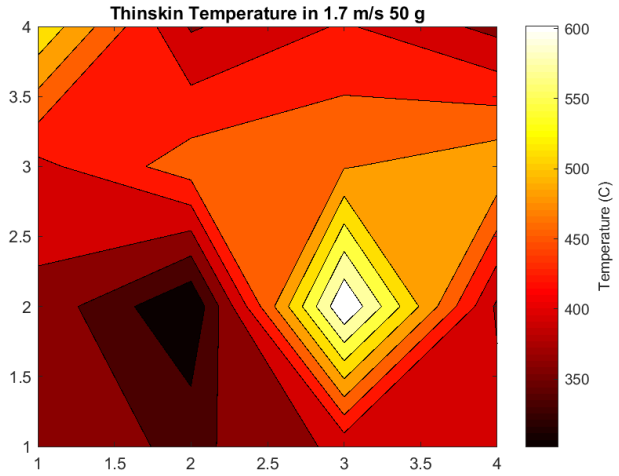

Figure 7.31: TSC data for wind speed of 1.4 m/s when 16 g firebrand were deposited.

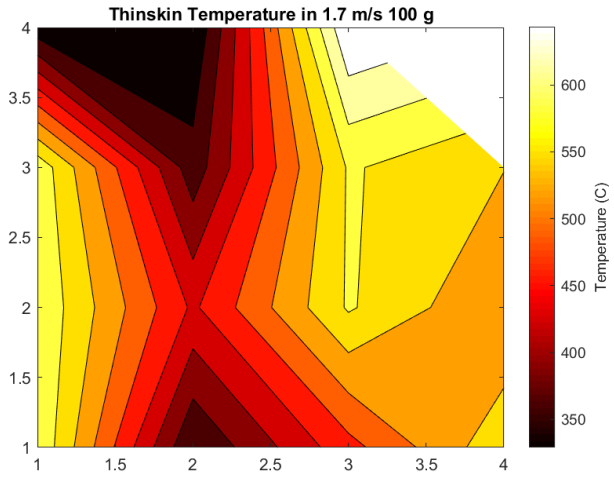

7.3. Few samples of Ignition Tests Results-TC data

Figure 7.32: TC data for plywood when 16 g firebrands were deposited and wind speed was 0.8 m/s.

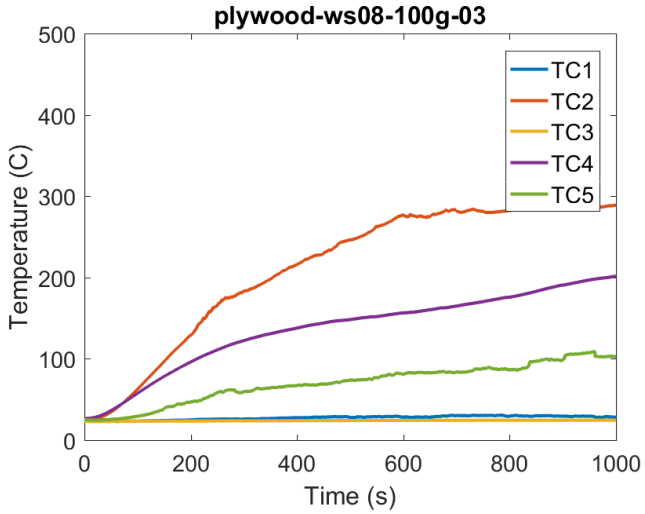

Figure 7.33: TC data for plywood when 16 g firebrands were deposited and wind speed was 1 m/s.

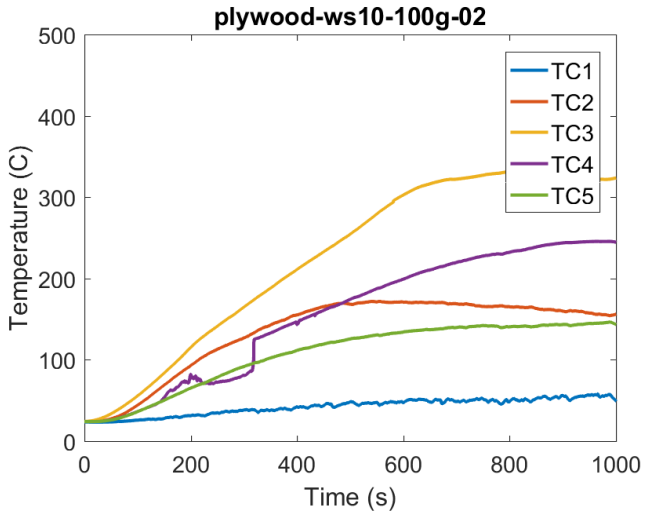

Figure 7.34: TC data for Cedar when 16 g firebrands were deposited and wind speed was 0.8 m/s.

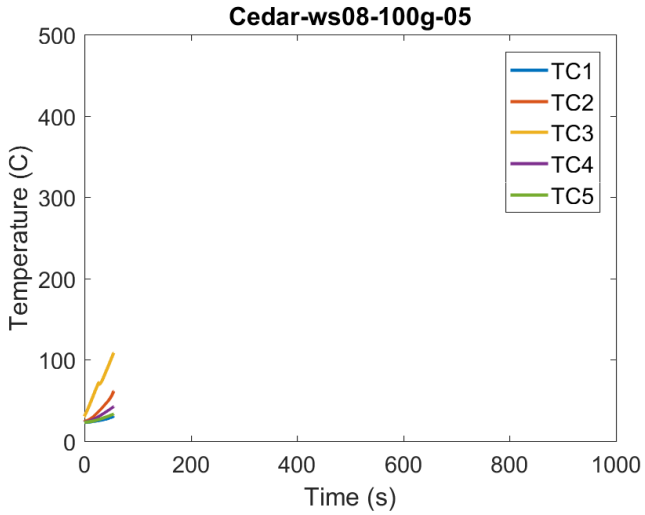

Figure 7.35: TC data for Cedar when 16 g firebrands were deposited and wind speed was 0.5 m/s.

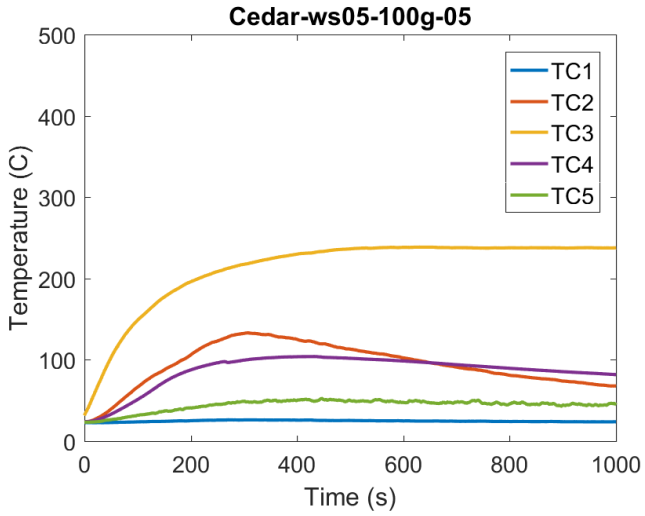

Figure 7.36: TC data for Cedar when 16 g firebrands were deposited and wind speed was 0.8 m/s.

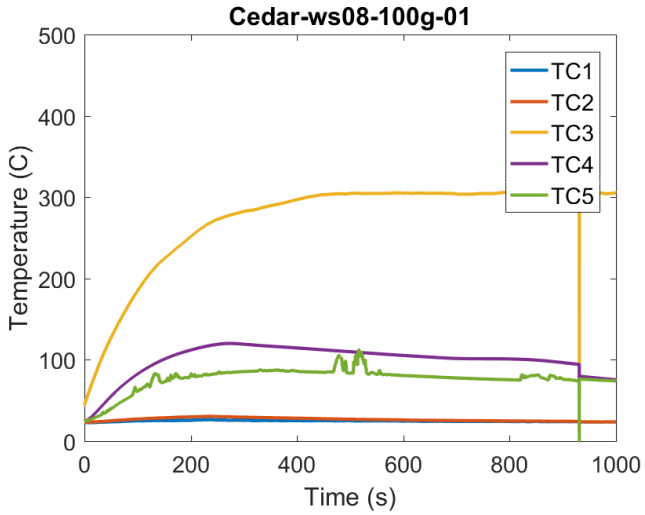

Figure 7.37: TC data for OSB when 16 g firebrands were deposited and wind speed was 0.5 m/s.

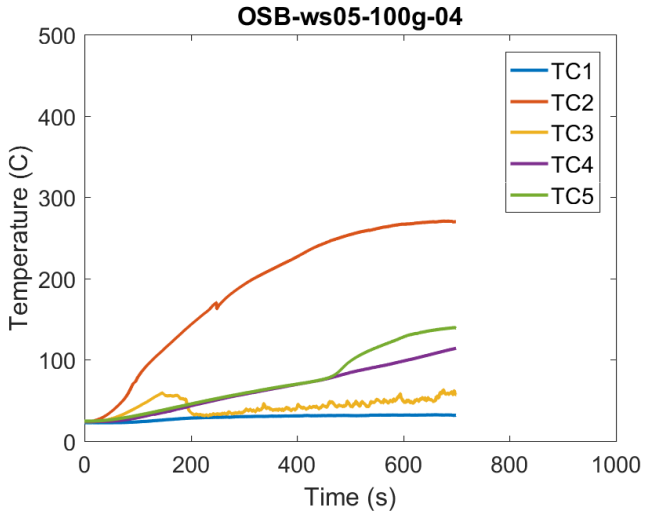

Figure 7.38: TC data for OSB when 16 g firebrands were deposited and wind speed was 0.8 m/s.

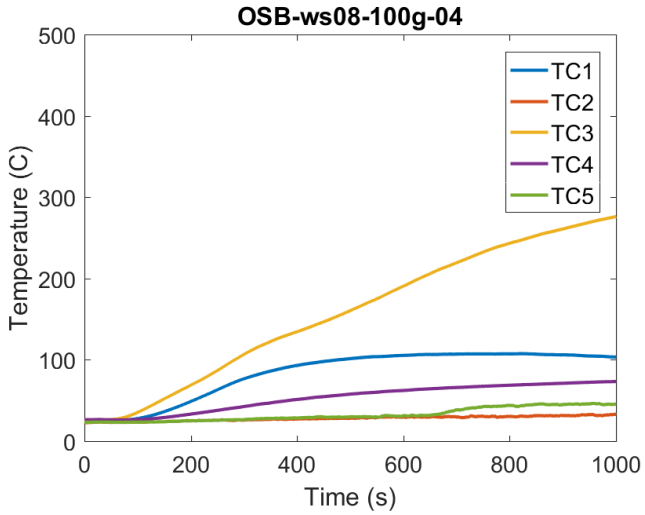

Figure 7.39: TC data for OSB when 16 g firebrands were deposited and wind speed was 1.2 m/s.

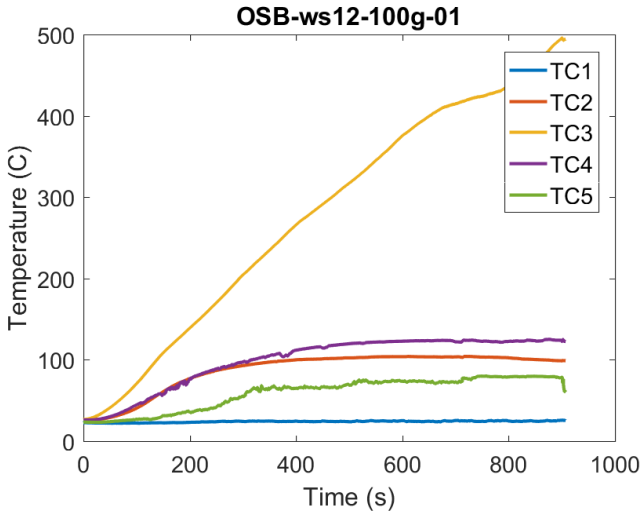
OSB-ws12-100g-01
Temperature (C)
Time (s)
TC1
TC2
TC3
TC4
TC5
0
100
200
300
400
500
0
200
400
600
800
1000

7.4. Table of all tests performed

Experiment List				
No. Tests	Fuel Type	Wind Speed	Firebrand Type	Deposited Mass
4	Sensor array	0.5 m/s	Birch (vendor1)	16 g
5	sensor array	0.8 m/s	Birch (vendor1)	16 g
12	sensor array	1.2 m/s	Birch (vendor1)	16 g
7	sensor array	1.4 m/s	Birch (vendor1)	16 g
5	sensor array	0.5 m/s	Birch (vendor1)	8 g
8	sensor array	0.8 m/s	Birch (vendor1)	8 g
7	sensor array	1.2 m/s	Birch (vendor1)	8 g
5	sensor array	1.4 m/s	Birch (vendor1)	8 g
5	sensor array	0.5 m/s	Birch (vendor1)	4 g
5	sensor array	0.8 m/s	Birch (vendor1)	4 g
5	sensor array	1.2 m/s	Birch (vendor1)	4 g
5	sensor array	1.4 m/s	Birch (vendor1)	4 g
3	sensor array	0.5 m/s	Birch (vendor2)	10 g
3	sensor array	0.5 m/s	Birch (vendor2)	16 g
5	sensor array	0.5 m/s	Birch (vendor2)	8 g
5	sensor array	0.8 m/s	Birch (vendor2)	8 g
5	sensor array	1.2 m/s	Birch (vendor2)	8 g
5	sensor array	1.4 m/s	Birch (vendor2)	8 g
5	sensor array	0.5 m/s	Birch (vendor2)	4 g
5	sensor array	0.8 m/s	Birch (vendor2)	4 g
5	sensor array	1.2 m/s	Birch (vendor2)	4 g
5	sensor array	1.4 m/s	Birch (vendor2)	4 g
5	sensor array	0.5 m/s	Birch (Oak)	8 g
3	sensor array	0.5 m/s	Birch (Oak)	4 g
3	sensor array	0.8 m/s	Birch (Oak)	4 g
3	sensor array	1.2 m/s	Birch (Oak)	4 g
3	sensor array	1.4 m/s	Birch (Oak)	4 g
4	Plywood	0.5 m/s	Birch (vendor1)	16 g
5	Plywood	0.8 m/s	Birch (vendor1)	16 g
5	Plywood	0.9 m/s	Birch (vendor1)	16 g
5	Plywood	1 m/s	Birch (vendor1)	16 g
10	Plywood	1.2 m/s	Birch (vendor1)	16 g
5	Plywood	1.4 m/s	Birch (vendor1)	16 g

Experiment List				
No. Tests	Fuel Type	Wind Speed	Firebrand Type	Deposited Mass
5	Plywood	0.5 m/s	Birch (vendor1)	8 g
3	Plywood	0.8 m/s	Birch (vendor1)	8 g
8	OSB	0.5 m/s	Birch (vendor1)	16 g
12	OSB	0.8 m/s	Birch (vendor1)	16 g
5	OSB	0.9 m/s	Birch (vendor1)	16 g
5	OSB	1 m/s	Birch (vendor1)	16 g
13	OSB	1.2 m/s	Birch (vendor1)	16 g
7	OSB	1.4 m/s	Birch (vendor1)	16 g
3	OSB	0.5 m/s	Birch (vendor1)	8 g
3	OSB	0.8 m/s	Birch (vendor1)	8 g
8	Cedar	0.5 m/s	Birch (vendor1)	16 g
8	Cedar	0.8 m/s	Birch (vendor1)	16 g
7	Cedar	0.9 m/s	Birch (vendor1)	16 g
3	Cedar	1 m/s	Birch (vendor1)	16 g
3	Cedar	1.2 m/s	Birch (vendor1)	16 g
3	Cedar	1.4 m/s	Birch (vendor1)	16 g

References

[1] Chris Lautenberger Rory M. Hadden, Sarah Scott and A. Carlos Fernandez-Pello. Ignition of combustible fuel beds by hot particles: An experimental and theoretical study. pages 341–355, 2010.

[2] Alexander Maranghides Sayaka Suzuki, Erik Johnsson and Samuel L. Manzello. Ignition of wood fencing assemblies exposed to continuous wind-driven firebrand showers. pages 1051–1067, 2016.

[3] E. Hakes R S P. Gorham D J. Zhou A. Gollner M J Caton, S. Review of pathways for building fire spread in the wildland urban interface part i: Exposure conditions. *Fire Technology*, pages 429–473, 2016.

[4] R.B. Hammer S.I.Stewart J.S.Fried S.S.Holcomb J.F.McKeefry Radelo, V.C. The wildland-urban interface in the united states. pages 799–805, 2005.

[5] Romme W Theobald D. Expansion of the u.s. wildland-urban interface. 83: 340–354, 2007.

[6] Cohen J. The wildland-urban interface problem. pages 22–26, 2008.

[7] National interagency coordination center. wildland fire summary and statis- tics annual report. 2016.

[8] A.I. Filkov E.L. Loboda V.V. Reyno A.V. Kozlov V.T. Kuznetsov D.P. Kasymov S.M. Andreyuk A.I. Ivanov Grishin, A.M and N.D. Stolyarchuk. A field experiment on grass fire effects on wooden constructions and peat layer ignition. pages 445–449, 2014.

[9] J. Cohen. Relating flame radiation to home ignition using modeling and experimental crown fires. pages 1616–1626, 2004.

[10] S.L. Manzello A. Maranghides D. Butry Mell, W.E. and R.G. Rehm. The wildland-urban interface problem current approaches and research needs. pages 238–251, 2010.

[11] D. McNamara W. Mell J. Trook Maranghides, A. and B. Toman. A case study of a community affected by the witch and guejito fires: Report 2 evaluating the effects of hazard mitigation actions on structure ignitions. pages 71–88, 2013.

[12] Samuel L Manzello, Seul-Hyon Park, and Thomas G Cleary. Investigation on the ability of glowing firebrands deposited within crevices to ignite common building materials. *Fire Safety Journal*, pages 894–900, 2009.

[13] M. J. Weston-Dawkes M. J. Gollner R. S. P. Hakes, H. Salehizadeh. Thermal characterization of firebrand piles. *Fire Safety Journal*, 2018.

[14] R.S.P. Hakes, H. Salehizadeh, M.J. Weston-Dawks, and M.J. Gollner. Thermal characterization of firebrand piles. *Fire Safety Journal*, 104:34–42, 2018.

[15] Guillermo Rein. Smoldering combustion. In *SFPE Handbook of Fire Protection Engineering, Fifth Edition*, pages 581–603. 2016. ISBN 9781493925650. doi: 10.1007/978-1-4939-2565-$0_1$9.

[16] RA Anthenien and AC Fernandez-Pello. A study of forward smolder ignition of polyurethane foam. In *Symposium (International) on Combustion*, volume 27, pages 2683–2690. Elsevier, 1998.

[17] James G. Quintiere. *Fundamentals of fire phenomena*. John Wiley and Sons, England, 2006.

[18] Thomas J Ohlemiller. Forced smolder propagation and the transition to flaming in cellulosic insulation. *Combustion and Flame*, 81(3-4):354–365, 1990.

[19] D Tse Stephen, A Carlo, Ferna Nde-Pello, and Kenji Miyasaka. Controlling mechanisms in the transition from smoldering to flaming of flexible polyurethane foam. In *Symposium (International) on Combustion*, volume 26, pages 1505–1513. Elsevier, 1996.

[20] Amnon Bar-Ilan, OM Putzeys, Guillermo Rein, A Carlos Fernandez-Pello, and

David L Urban. Transition from forward smoldering to flaming in small polyurethane foam samples. *Proceedings of the Combustion Institute*, 30(2):2295–2302, 2005.

[21] Amanda B Dodd, Christopher Lautenberger, and Carlos Fernandez-Pello. Computational modeling of smolder combustion and spontaneous transition to flaming. *Combustion and Flame*, 159(1):448–461, 2012.

[22] James L Urban, Casey D Zak, and Carlos Fernandez-Pello. Spot fire ignition of natural fuels by hot aluminum particles. *Fire technology*, 54(3):797–808, 2018.

[23] James L Urban, Casey D Zak, Jiayun Song, and Carlos Fernandez-Pello. Smoldering spot ignition of natural fuels by a hot metal particle. *Proceedings of the Combustion Institute*, 36(2):3211–3218, 2017.

[24] James L Urban, Casey D Zak, and Carlos Fernandez-Pello. Cellulose spot fire ignition by hot metal particles. *Proceedings of the Combustion Institute*, 35(3):2707–2714, 2015.

[25] AC Fernandez-Pello, C Lautenberger, D Rich, C Zak, J Urban, R Hadden, S Scott, and S Fereres. Spot fire ignition of natural fuel beds by hot metal particles, embers, and sparks. *Combustion science and technology*, 187(1-2):269–295, 2015.

[26] CASEY Zak, JAMES Urban, V Tran, and AC Fernandez-Pello. Flaming ignition

behavior of hot steel and aluminum spheres landing in cellulose fuel beds. *Fire Safety Science*, 11:1368–1378, 2014.

[27] Haixiang Chen Supan Wang, Xinyan Huang and Naian Liu. Interaction between flaming and smouldering in hot-particle ignition of forest fuels and effects of moisture and wind. pages 71–88, 2017.

[28] Haixiang Chen Jesse S. Lozano-Yanlong Shan Panpan Yin, Naian Liu. New correlation between ignition time and moisture content for pine needles attacked by firebrands. pages 71–88, 2012.

[29] Thomas G. Cleary John R. Shields Samuel L. Manzellon, y and Jiann C. Yang. On the ignition of fuel beds by firebrands. pages 77–87, 2001.

[30] Samuel L Manzello, Thomas G Cleary, John R Shields, and Jiann C Yang. Ignition of mulch and grasses by firebrands in wildland–urban interface fires. *International Journal of Wildland Fire*, 15(3):427–431, 2006.

[31] M. Almeida J. Raposo R. Oliveria Viegas, D.X. and C.X. Viegas. Ignition of mediterranean fuels beds by several types of firebrands. pages 60–77, 2014.

[32] PFM Ellis. The likelihood of ignition of dry-eucalypt forest litter by firebrands. *International Journal of Wildland Fire*, 24(2):225–235, 2015.

[33] Alok Warey. Influence of thermal contact on heat transfer from glowing firebrands. pages 301–311, 2018.

[34] T.E. Waterman and A.N. Takata. Laboratory study of ignition of host mate- rials by firebrands. 1969.

[35] S. Manzello. Enabling the Investigation of Structure Vulnerabilities to Wind-Driven Firebrand Showers in Wildland-Urban Interface (WUI) Fires. *Fire Safety Science*, 11:83–96, 2014. ISSN 18174299. doi: 10.3801/IAFSS.FSS.11-83. URL http://www.iafss.org/publications/fss/11/83.

[36] Samuel L. Manzello, Yoshihiko Hayashi, Takefumi Yoneki, and Yu Yamamoto. Quantifying the vulnerabilities of ceramic tile roofing assemblies to ignition during a firebrand attack. *Fire Safety Journal*, 45(1):35–43, jan 2010. ISSN 03797112. doi: 10.1016/j.firesaf.2009.09.002. URL http://linkinghub.elsevier.com/retrieve/pii/S0379711209001192.

[37] Samuel L. Manzello, Sayaka Suzuki, and Yoshihiko Hayashi. Enabling the study of structure vulnerabilities to ignition from wind driven firebrand showers: A summary of experimental results. *Fire Safety Journal*, 54:181–196, nov 2012. ISSN 03797112. doi: 10.1016/j.firesaf.2012.06.012. URL http://linkinghub.elsevier.com/retrieve/pii/S0379711212000847.

[38] Sayaka Suzuki, Samuel L. Manzello, Koji Kagiya, Junichi Suzuki, and Yoshihiko Hayashi. Ignition of Mulch Beds Exposed to Continuous Wind-Driven Firebrand Showers. *Fire Technology*, 51(4): 905–922, jul 2015. ISSN 0015-2684. doi: 10.1007/s10694-014-0425-2. URL http://dx.doi.org/10.1007/s10694-014-0425-2 http://link.springer.com/10.1007/s10694-014-0425-2.

[39] Samuel L Manzello, John R Shields, Yoshihiko Hayashi, and Daisaku Nii. Investigating the vulnerabilities of structures to ignition from a firebrand attack. *Fire Safety Science*, pages 143–154, 2008. ISSN 18174299. doi: 10.3801/IAFSS.FSS.9-143.

[40] Samuel L Manzello and Sayaka Suzuki. Exposing decking assemblies to continuous wind-driven firebrand showers. *FIRE SAFETY SCIENCE-PROCEEDINGS OF THE ELEVENTH INTERNATIONAL SYMPOSIUM*, pages 1339–1352, 2014.

[41] A ASTM D4442. Standard test methods for direct moisture content measurement of wood and wood-based materials, 2016.

[42] ASTM. ASTM E459 - Thin Skin Calorimeter.

[43] Cowlard A. Abecassis-Empis C. Krajcovic M. Torero J.L. Hidalgo J.P., Maluk C. A thin-skin calorimeter (tsc) for quantifying irradiation during large-scale fire testing. 112:383–394, 2016.

[44] Vytenis Babrauskas. Development of the cone calorimetera bench-scale heat release rate apparatus based on oxygen consumption. *Fire and Materials*, 8(2):81–95, 1984.

[45] James L Urban, Michela Vicariotto, Derek Dunn-Rankin, and A Carlos Fernandez-Pello. Temperature measurement of glowing embers with color pyrometry. *Fire Technology*, pages 1–14, 2019.

[46] Vytenis Babrauskas. Ignition of wood a review of the state of the art. pages 71–88, 2001.

[47] Li Yudong and Dougal Drysdale. Measurement of the ignition temperature of wood. 1:380–385, 1992.